

Award Number: **W81XWH-08-1-0701**

TITLE: **Micro and Nano-mediated 3D Cardiac Tissue Engineering**

PRINCIPAL INVESTIGATOR:

- **Rashid Bashir, PhD, PI**
- **Brian Cunningham, PhD, co-PI**
- **Hyunjoon Kong, PhD, co-PI**
- **Taher Saif, PhD, co-PI**
- **Larry Schook, PhD, co-PI**

CONTRACTING ORGANIZATION:

University of Illinois , Champaign, IL 61820

REPORT DATE: **October 2009**

TYPE OF REPORT: **Annual**

PREPARED FOR: U.S. Army Medical Research and Materiel Command
Fort Detrick, Maryland 21702-5012

DISTRIBUTION STATEMENT:

Approved for public release; distribution unlimited

The views, opinions and/or findings contained in this report are those of the author(s) and should not be construed as an official Department of the Army position, policy or decision unless so designated by other documentation.

REPORT DOCUMENTATION PAGE

Form Approved
OMB No. 0704-0188

Public reporting burden for this collection of information is estimated to average 1 hour per response, including the time for reviewing instructions, searching existing data sources, gathering and maintaining the data needed, and completing and reviewing this collection of information. Send comments regarding this burden estimate or any other aspect of this collection of information, including suggestions for reducing this burden to Department of Defense, Washington Headquarters Services, Directorate for Information Operations and Reports (0704-0188), 1215 Jefferson Davis Highway, Suite 1204, Arlington, VA 22202-4302. Respondents should be aware that notwithstanding any other provision of law, no person shall be subject to any penalty for failing to comply with a collection of information if it does not display a currently valid OMB control number. **PLEASE DO NOT RETURN YOUR FORM TO THE ABOVE ADDRESS.**

1. REPORT DATE (DD-MM-YYYY) 01-10-2009		2. REPORT TYPE Annual		3. DATES COVERED (From - To) 24 Sep 2008 - 23 Sep 2009	
4. TITLE AND SUBTITLE Micro and Nano-mediated 3D Cardiac Tissue Engineering				5a. CONTRACT NUMBER	
				5b. GRANT NUMBER W81XWH-08-1-0701	
				5c. PROGRAM ELEMENT NUMBER	
6. AUTHOR(S) <ul style="list-style-type: none"> • Rashid Bashir, PhD, PI • Co-PIs: Brian Cunningham, Hyunjoon Kong, Taher Saif, and Larry Schook 				5d. PROJECT NUMBER	
				5e. TASK NUMBER	
				5f. WORK UNIT NUMBER	
7. PERFORMING ORGANIZATION NAME(S) AND ADDRESS(ES) University of Illinois Champaign, IL 61820				8. PERFORMING ORGANIZATION REPORT NUMBER	
9. SPONSORING / MONITORING AGENCY NAME(S) AND ADDRESS(ES) U.S. Army Medical Research and Materiel Fort Detrick, Maryland 21702-5012				10. SPONSOR/MONITOR'S ACRONYM(S)	
				11. SPONSOR/MONITOR'S REPORT NUMBER(S)	
12. DISTRIBUTION / AVAILABILITY STATEMENT Approved for public release; distribution unlimited					
13. SUPPLEMENTARY NOTES					
14. ABSTRACT The project envisages to improve the care of battlefield-related cardiac injuries by providing novel methods to design and fabricate 3-D models of cardiac sub-components that would be critical in restoring the function of the heart. We successfully established a rat breeding colony according to IACUC protocols and isolated neonatal rat ventricular myocytes in culture (>80% viability). These cells are being shared among all subgroups for future studies. We examined the effects of substrate stiffness on the beating rate and beating force in embryonic chicken cardiac myocytes. Our results showed that cells cultured on polyacrylamide (PA) substrates had elasticity comparable to that of native myocardium exhibiting the highest beating rate. We also successfully mobilized peripheral blood stem cells and collected large numbers of cells via leukapheresis in the pig model. We are continuing work on the characterization portion of year one Milestone 8. We have synthesized the biodegradable methacrylic alginate (MA) and used it to control the elastic modulus and degradation rate in an independent manner. The hydrogel cross-linked with hydrolytically labile oxidized methacrylic alginate was used as a VEGF-releasing device, which stimulated the capillary blood vessel growth. We also undertook the development of label-free imaging of cell adhesion to surfaces using Distributed Feedback Laser Biosensor (DFBLB) surfaces and related detection instruments.					
15. SUBJECT TERMS Biomaterials, Biosensors, Fabrication, Mechanobiology					
16. SECURITY CLASSIFICATION OF: U			17. LIMITATION OF ABSTRACT UU	18. NUMBER OF PAGES 39	19a. NAME OF RESPONSIBLE PERSON USAMRMC
a. REPORT U	b. ABSTRACT U	c. THIS PAGE U			19b. TELEPHONE NUMBER (include area code)

Table of Contents

Contents

SECTION I: Annual Report Overall Project.....	5
I. Summary of Work	5
II. INTRODUCTION	5
IV. KEY RESEARCH ACCOMPLISHMENTS.....	7
V. REPORTABLE OUTCOMES.....	8
VI. CONCLUSION.....	9
SECTION II: Annual Report from Project Subgroups.....	9
Appendix: Publications	33

SECTION I: Annual Report Overall Project

This section describes briefly the salient aspects of the research for the 2008-09 period. Additional details about sub-tasks are provided in subsequent sections.

I. Summary of Work

We successfully established a rat breeding colony according to IACUC protocols and isolated neonatal rat ventricular myocytes in culture (>80% viability). These cells are being shared among all subgroups for future studies. We examined the effects of substrate stiffness on the beating rate and beating force in embryonic chicken cardiac myocytes. Our results showed that cells cultured on polyacrylamide (PA) substrates had elasticity comparable to that of native myocardium exhibiting the highest beating rate.

We also successfully mobilized peripheral blood stem cells and collected large numbers of cells via leukapheresis in the pig model. We are continuing work on the characterization portion of year one Milestone 8. We have synthesized the biodegradable methacrylic alginate (MA) and used it to control the elastic modulus and degradation rate in an independent manner. The hydrogel cross-linked with hydrolytically labile oxidized methacrylic alginate was used as a VEGF-releasing device, which stimulated the capillary blood vessel growth. We also undertook the development of label-free imaging of cell adhesion to surfaces using Distributed Feedback Laser Biosensor (DFBLB) surfaces and related detection instruments.

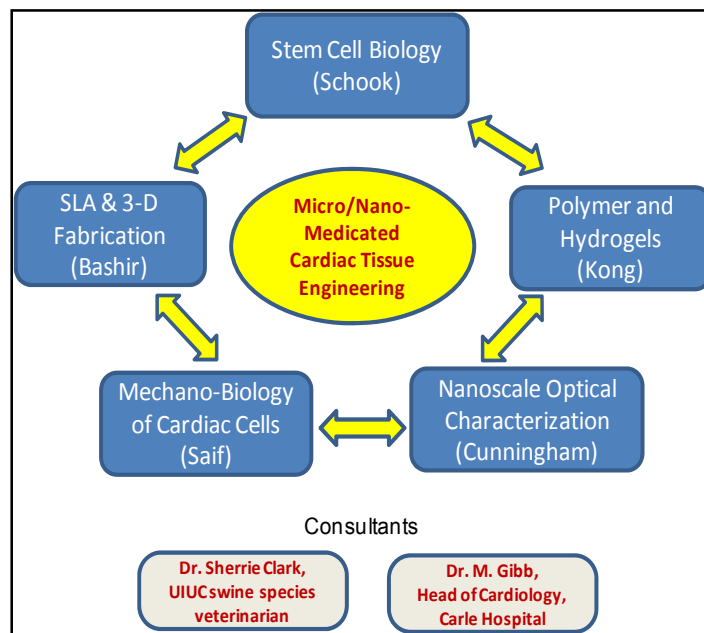
II. INTRODUCTION

The regeneration of cells and tissue after injury or trauma is critical to medical and civilian communities. Cardiac injuries and regenerative engineering poses specific challenges since cardiac myocytes, the primary cells responsible for the mechanical beating of the heart muscle, do not regenerate. The cardiac system poses a significantly challenging problem in tissue engineering due to the complex 3-dimensional mechano-actuation properties of the cardiac cells. A grand challenge in cardiology since early 50s is the development of an artificial heart that can replace a failing heart. Until today, artificial heart is used only for the temporary use (hrs) until a healthy donor heart is found. The latter is difficult to get, and is often rejected by the body after successful replacement. This very limited success in heart replacement, in spite of considerable effort and resources invested so far, calls for a new paradigm in the approach of heart replacement. This project attempts to offer such a paradigm by proposing to "grow" the heart or its components from the basic building blocks, namely the cells (differentiated cardiomyocytes) of the patient, biomaterials design, namely the hydrogel scaffolds to house the cells, and nanotechnology, namely the stereo-lithographically-patterned 3D substrate. New knowledge on cells' response to mechanical cues, and recent findings on cardiomyocyte functionality on mechanically tuned substrates from our labs form the basis for the project. In summary, stem cell differentiation in scaffolds, novel 3-D fabrication technologies, use of the appropriate biomaterials, integration of peptides for cardiac cell attachment and cell growth, the characterization of the scaffold materials and the transmembrane proteins, and cardiac cell

mechanics are all critical elements of a comprehensive design approach proposed in this project for 3-D cardiac tissue engineering.

This project offers a paradigm by proposing to "grow" the heart or its components from the basic building blocks, the cells (differentiated cardiomyocytes) of the patient, biomaterials design of the hydrogel scaffolds to house the cells, use of 3-D stereolithography for fabricating the hydrogel scaffolds with cardiac cells, and nanoscale mechanical and optical tools for characterization of cardiac cells and their interactions with the scaffolds. Our objectives are to integrate these multi-disciplinary efforts and develop the strategies and methodologies for novel designs of 3-D components of an artificial heart.

The project overview and research thrusts for each of the co-PIs is provided in the figure below, and the following table enlists first year project goals:.



Year 1 Project Goals	
1	Design and fabricate DFB laser biosensor structures and scanning detection instrument with 3-5 micron spatial resolution using a focused pump beam and a conventional scanning motor stage.
2	Develop capability for exciting DFB emission using a near-field scanning probe tip.
3	To demonstrate and characterize the capability of using SL as a means to scale-up or improve the throughput of our tissue fabrication.
4	To demonstrate biologically-relevant 3-D scaffold structures and percent cell viability versus time in confocal microscopy
5	Synthesize bioactive, biodegradable acrylic alginates, demonstrate hydrogel fabrication with SLA
6	Develop/characterize (AFM) 2D variable stiffness substrate w/ patterns of high stiff regions.
7	Functionalize the surface with fibronectin, laminin, and collagen and characterize their density.

III. BODY

Potential Military Relevance. Battlefield trauma resulting in a variety of injuries is of significant concern to our military and civilian administration. Tissue engineering or regenerative medicine offers viable alternatives to counter many such injuries. Our project envisages to improve the care of battlefield-related cardiac injuries by providing novel methods to design and fabricate 3-D models of cardiac sub-components that would be critical in restoring the function of the heart. According to the report on 'Capturing the power of biomaterials for military medicine'(NRC Report,2004), four areas in which enhancement of biomaterials and biotechnology will have a major impact on acute, chronic, and rehabilitation care in military medicine are (1) wound care, (2) tissue engineering, (3) drug delivery, and (4) physiological sensors and diagnostics. Our target area of research in cardiac tissue engineering, addresses one of the critical needs for the care in military medicine. The ultimate goals of our research are to resolve chronic medical problems and ultimate rehabilitation of injured military personnel (NRC Report, 2004). Our approach of using a mobilized cell population also provides flexibility in obtaining human MSCs in the field. They could be harvested from the soldiers and banked so they would have a source of their own cells. This approach is much faster and safer than bone marrow derived cells. The scaffolds we will develop could also be loaded with drugs that would be released over time to allow minimizing rejection by the body. Clearly, new methods for development of engineered tissues will have many applications beyond cardiac tissue engineering to engineering of vessels, skin, and many other organs.

IV. KEY RESEARCH ACCOMPLISHMENTS

- Hydrogel formulation to decouple the dependency of gel stiffness on the swelling ratio
- Demonstration of improved cell viability and cellular VEGF secretion with methacrylic alginate
- Developed 3-D SL process with 'top down' and 'bottoms up' approach for multiple cell types
 - To date with PEG1000, moving to PEGDA-700 + MA
- Mechanical design guidelines for stiffness and insight into mechanical cell communication
- Novel label free imaging method for cell-substrate interactions
- Stem cell extraction protocols and pig infarction model developed

V. REPORTABLE OUTCOMES

List of Publication Accepted by Peer-Reviewed Journals

- Cha, C., Kohman, R., & Kong, H.J. Biodegradable Polymer Cross-linker: Independent Control of Stiffness, Toughness and Degradation Rate of Hydrogel. *Advanced Functional Materials* 19; 1-7 (2009).

Conference Presentations

- Cha, C. & Kong, H.J. Biodegradable polymeric crosslinker: Independent control of mechanics and degradation, Oral presentation at the American Chemical Society (ACS) meeting, Washington DC, Aug. 2009
- Chan, V., Jeong, J., Bajaj, P., Kong, H., and Bashir, R., "Three-Dimensional Hydrogel Fabrication Using Stereolithography for Live Cell Encapsulation", 2009 Biomedical Engineering Society Annual Fall Meeting, Pittsburgh, October 7-10, 2009.
- Jeong, J., Chan, V., Cha, C., Bashir, R., and Kong, H., "In situ Cell Encapsulation into a Vascularized Hydrogel Matrix Using Stereolithography", 2009 Biomedical Engineering Society Annual Fall Meeting, Pittsburgh, October 7-10, 2009.
- Bajaj, P., Tang, X., Saif, T., Bashir, R., "Substrate Stiffness Influence the Beating Rate and Beating Force of Embryonic Chicken Cardiac Myocytes", 2009 Biomedical Engineering Society Annual Fall Meeting, Pittsburgh, October 7-10, 2009.
- Bajaj, P., Akin, D., Bashir, R., "Cardiac cell based bio-batteries", 2009 Biomedical Engineering Society Annual Fall Meeting, Pittsburgh, October 7-10, 2009.

List of Manuscripts in Preparation

- Cha, C & Kong, H.J. Decoupled control of hydrogel stiffness and swelling behavior
- Cha, C. & Kong, H.J. Refined control of growth factor sequestration in a 3D hydrogel matrix
- Jeong, J. Chan, V., Bashir, R. & Kong, H.J. Vascularized hydrogel matrix using SLA processing
- Chu, C. & Kong, H.J. Biomimetic design of 3D ECM using methacrylic collagen
- Chan, V., Jeong, J., Kong, H. J., & Bashir, R. Stereolithography based 3D Cell-laden scaffolds using top-down and bottoms up fabrication
- Tang, X., Bajaj, P., Bashir, R., Saif, M. T. A., Dependence of cardiac cell beating and force on substrate stiffness

VI. CONCLUSION

We have created a mild-conditioned process for encapsulating living cells in complex 3D scaffolds using stereolithography. This is a new tool that could potentially allow us to create thicker tissue by fabricating artificial vascular networks. We also showed that the beating rate of embryonic chicken cardiac myocytes depended on the stiffness of the substrate only during the first few days of culture. Subsequently, there was a convergence of the beating rate possibly due to mechanical coupling between the cells mediated by the soft substrate or proliferating fibroblasts that bridged between the cells. Our results also showed that the beating force by cardiac cells was consistently greater on the rigid polystyrene substrate, most likely because of the formation of very stable focal adhesion complexes compared to few dynamic focal adhesion complexes on soft PA gels. We created and characterized an anti-porcine CD34 antibody capable of recognizing the antigen in both flow cytometry and Western Blot applications. The CD34 antigen is important in stem cell research due to its widespread use in identifying stem cell subsets in a variety of tissues, and are important current clinical trials exploring the use of CD34+ cell subsets for therapies following myocardial infarction. The importance of this reagent in the pig model is the widespread use of swine for cardiac research.

The incorporation of oxidized methacrylic alginate into a poly(ethylene glycol) hydrogel allowed us to control the mechanical properties, swelling ratio and degradation rates in an independent manner. The independent control of mechanical properties and degradation rates of a hydrogel enabled the refined control of angiogenic growth factor release and subsequently improve the capillary blood vessel formation. The biosensor surface can be prepared with hydrogels that are being considered for the 3D cell scaffold, and used as a tool for evaluating the attachment, growth, and differentiation of cells.

SECTION II: Annual Report from Project Subgroups

Research Group: Rashid Bashir

Period Aug'08 to Aug'09

I. Summary of Work

We have successfully established a rat breeding colony according to IACUC protocols and isolated neonatal rat ventricular myocytes in culture (>80% viability). These cells will be shared among all subgroups in future studies. During that time span, we have also procured the stereolithography apparatus and successfully adapted it for use with specific tissue engineering applications. NIH/3T3 murine fibroblasts were encapsulated in poly(ethylene glycol) hydrogels with photosensitive acrylate groups using stereolithography. Our bottoms-up approach yields cell-laden, homogeneous scaffolds at high densities that conform to the three-dimensional geometries specified in the computer. With our approach, we have also layered multi-cell types in patterns that are 100- μ m thick intervals. We are continuing work on long-term cell viability studies using an assortment of photosensitive hydrogels at our disposal.

II. INTRODUCTION

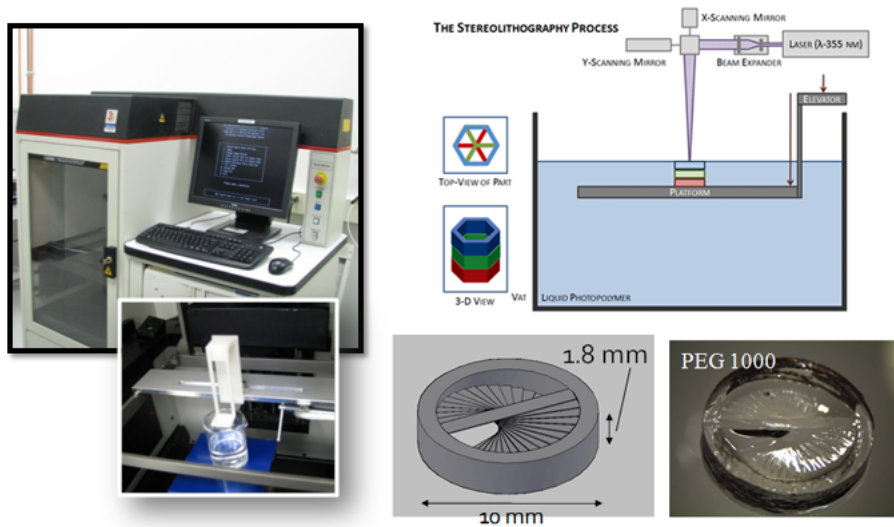
The goal of the Bashir subgroup is to demonstrate and characterize the capability of using the stereolithography to design and generate complex 3-D tissue with tunable architecture. The cell type that we are ultimately interested in using is primary neonatal rat ventricular myocytes.

III. BODY

To demonstrate and characterize the capability of using stereolithography as a means to scale-up or improve the throughput of our tissue fabrication.

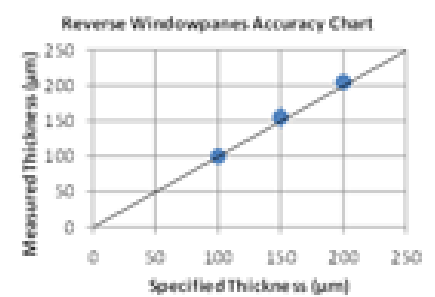
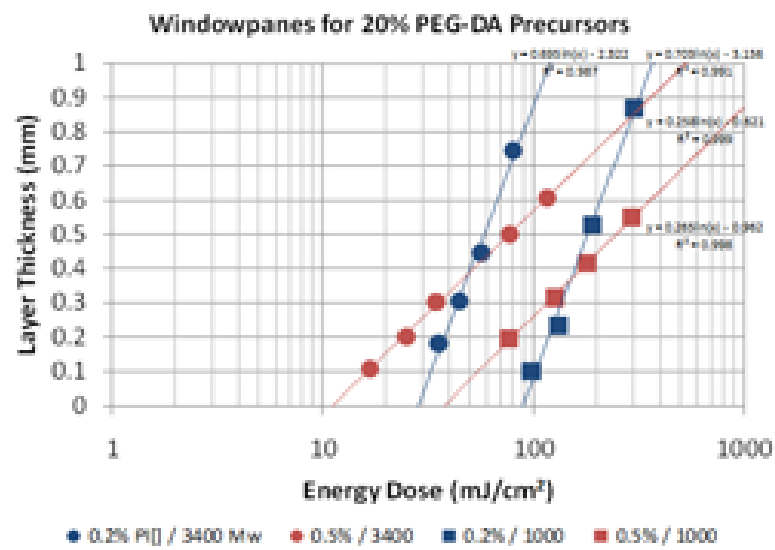
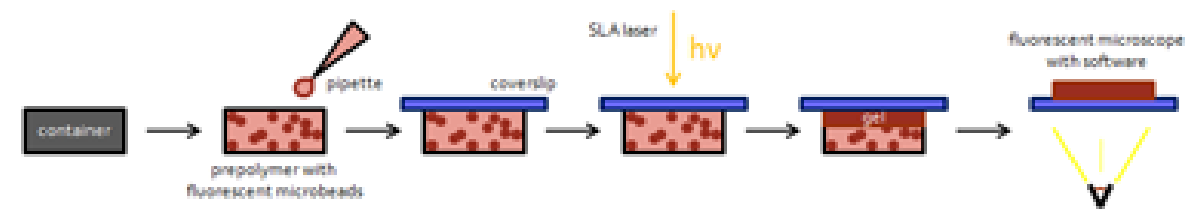
System modification

Stereolithography is a liquid rapid prototyping system, which uses ultraviolet light to create polymer structures. It is the first of a group of technologies that fabricate objects layer-by-layer from a computer-aided design (CAD) of the object. It makes fabricating higher-ordered structures with internal architecture possible without the difficulties of conventional scaffold fabrication techniques. Since the large volume that is required to operate the stereolithography system is impractical for use with living cells or photosensitive biomaterials, we modified the system by constructing a mini-platform that attaches to the elevator. This allows us to use much smaller volumes for cell encapsulation.

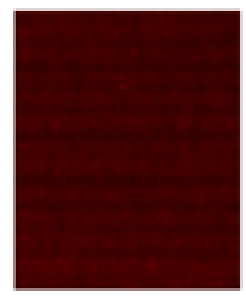
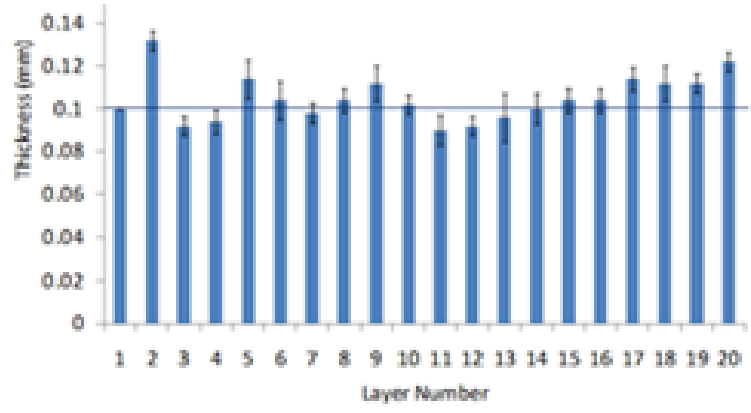


Creating complex 3D structures in the stereolithography requires the photosensitive material properties to be carefully characterized as it relates to the laser. These parameters are described in the equation, $C_d = D_p \ln \frac{E_{ave}}{E_c}$, where C_d is the cure depth, D_p is the penetration depth, E_{ave} is the average energy dose of the laser, and E_c is the critical energy dose required to form to turn the liquid pre-polymer into a cured gel. The constants, D_p and E_c , are material

properties that must be inputted into the system. We were able to calculate these constants by taking advantage of the transparent property of the hydrogel. Fluorescent microbeads (1- μm) were encapsulated in gels that were polymerized using different energy doses from the laser. This created gels of various thicknesses that were graphed on a semi-logarithmic plot. In the resulting line, D_p was the slope and E_c was the y-intercept. By characterizing these parameters carefully, we were able to create layers of precisely-defined thicknesses.

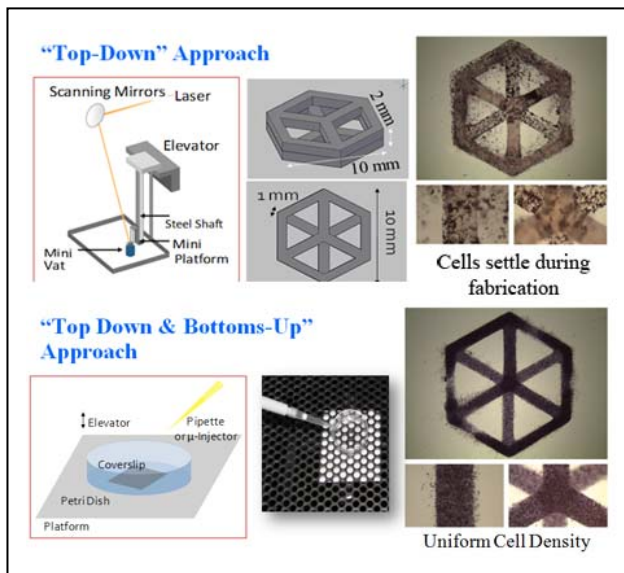


LAYER	THICKNESS (µm)	VOLUME (µL)
1 & 2	200	900
3	100	160
4	100	120
5	100	120
6+	100+	120

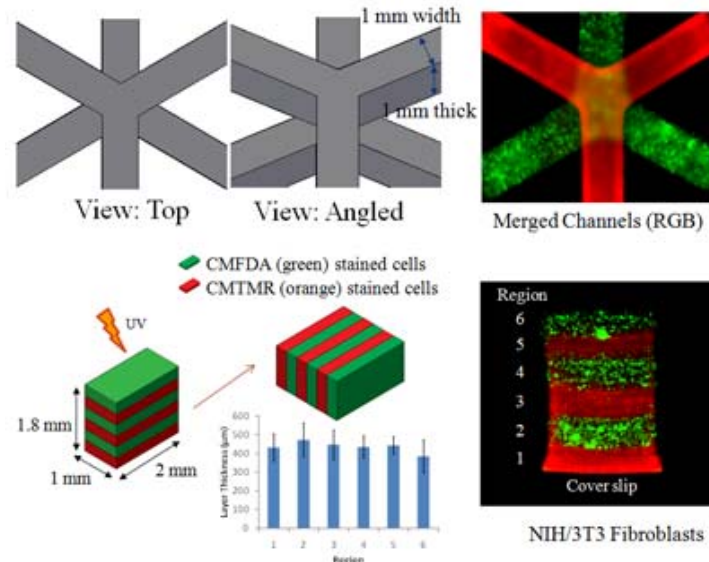


To demonstrate biologically-relevant 3-D scaffold structures in the confocal microscopy

By characterizing the photosensitive material carefully, we were then able to focus on encapsulating living cells in biologically-relevant 3-D scaffold structures. Using the “top-down” approach, we found out that cells in the pre-polymer solution tended to settle at the bottom of the container very quickly. This made it difficult to create uniform cell densities from layer to layer. The “bottoms-up” approach, in contrast, successfully produced uniform cell densities from the first to the last layer. This approach required manual pipetting after every layer.



There are many cell-encapsulation applications that can be derived from this technique. For example, many groups are studying the interaction of co-cultures in 3D. The ability to layer more multi-cell types in 3D can easily be performed in the stereolithography system (as shown below). The thicknesses of these structures can also be controlled (quantitative graph). NIH/3T3 murine fibroblasts were separated in two groups; each group was labeled with a different fluorescent CellTracker® dye: CMFDA (Green) and CMTMR (Red). The cells labeled in red dye were dispensed and polymerized first. This was followed by cells labeled in green dye and the process was repeated as desired. We are working on encapsulating cardiac myocytes in co-culture with fibroblasts (or adult stem cells).



IV. KEY RESEARCH ACCOMPLISHMENTS

- Procured and adapted stereolithography apparatus for low volume biological applications
- Developed 3-D process for developing PEG1000 hydrogel structures.
- Encapsulated multi-cell types in multi-layered hydrogel structures, which were visualized using epifluorescence and confocal microscopy
- Successfully established a rat breeding colony according to IACUC protocols and isolated neonatal rat ventricular myocytes in culture (>80% viability).

V. REPORTABLE OUTCOMES

- Conference presentation: Chan, V., Jeong, J., Bajaj, P., Kong, H., and Bashir, R., "Three-Dimensional Hydrogel Fabrication Using Stereolithography for Live Cell Encapsulation", 2009 Biomedical Engineering Society Annual Fall Meeting, Pittsburgh, October 7-10, 2009.
- Conference poster: Jeong, J., Chan, V., Cha, C., Bashir, R., and Kong, H., "In situ Cell Encapsulation into a Vascularized Hydrogel Matrix Using Stereolithography", 2009 Biomedical Engineering Society Annual Fall Meeting, Pittsburgh, October 7-10, 2009.
- Publication in preparation: Jeong, J. Chan, V., Bashir, R. & Kong, H.J. Vascularized hydrogel matrix using SLA processing
- Publication in preparation: Chan, V., Jeong, J., Kong, H. J., & Bashir, R. Stereolithography based 3D Cell-laden scaffolds using top-down and bottoms up fabrication

VI. CONCLUSION

We have created a mild-conditioned process for encapsulating living cells in complex 3D scaffolds using stereolithography. This is a new tool that could potentially allow us to create thicker tissue by fabricating artificial vascular networks. With this technique, we could also layer multi-cell types in the scaffold. This is important because tissues are composed of more than one cell-type. Studying the interaction between two or more cell types could help us understand the assembly and development of higher-ordered tissue. Using novel hydrogels such as methacrylic alginates, we could also vary the stiffness and bioactive properties of the scaffold to improve tissue functionality. Finally, we are continuing to work on incorporating primary cardiac myocytes to the encapsulation process.

Research Group: Taher Saif

Period Aug'08 to Aug'09

Annual Report from Project Subgroups

I. Summary of Work

We examined the effects of substrate stiffness on the beating rate and beating force in embryonic chicken cardiac myocytes. Our results show that cells cultured on polyacrylamide (PA) substrates with elasticity comparable to that of native myocardium exhibit the highest beating rate. Initial beating rate of individual cells on all the substrates varies greatly, but the standard deviation in frequency decreases significantly in a few days. During the same time, average frequency for all the substrates converge to a similar value. The beating force of the cardiac cells were quantified using a versatile micro-electromechanical system (MEMS) force sensor and it was found that the force for the cells cultured on stiff polystyrene culture plates ($F = 79.46 \pm 17.20$ nN) was consistently larger than those cultured on soft PA gels ($F = 30.16 \pm 3.83$ nN).

II. INTRODUCTION

It is well known that living cells can sense their mechanical microenvironment and respond to mechanical cues with changes in gene expression, cell morphology, cell migration, and cell division. Previous studies show that mesenchymal stem cells (MSCs) can differentiate to specific lineages/fates based on the stiffness of the substrates.¹ Neurons have been shown to display increased branched actin structures on soft brain-like substrates as compared to stiff substrates, whereas glial cells like astrocytes from the central nervous system (CNS) grow better on stiff substrates than on soft ones.² Fibroblasts have been shown to adjust their intercellular cell stiffness to match the stiffness of the substrate on which they are cultured.³

Moreover, when 3T3 fibroblasts were cultured on a substrate with varying rigidity along the surface, they readily migrated from the soft side of the substrate to the rigid side, termed “durotaxis”.⁴ Myoblasts, which are the precursors of myotubes, differentiate optimally and show actomyosin striations only on substrates with stiffness typical of a normal muscle.⁵ Stiffness of the substrate can also dictate whether a cell will grow or undergo apoptosis, and non-transformed NIH 3T3 fibroblasts cultured on soft substrates showed decrease in the rate of DNA synthesis and increase in the rate of apoptosis when compared to the same cells cultured on rigid substrates.⁶

The stiffness of the substrate/tissue also plays an important role in the development and the normal functioning of the myocardium.

III. BODY

Substrate Stiffness Influences the Beating Force of Embryonic Chicken Cardiac Myocytes

The effect of substrate stiffness on the beating force in embryonic chicken cardiac myocytes was examined in the current study. To mimic a wide range of physiological mechanical micro-environments, polyacrylamide (PA) gels with three different stiffness were produced. Soft PA gels with stiffness $1.05 (\pm 0.17)$ kPa were used to mimic mammary gland, brain and breast, which have psychological stiffness ranging from 0.1 to 2 kPa^{1,2}. Intermediate hard gels with stiffness $18.31 (\pm 0.19)$ kPa were used to mimic chicken embryonic myocardium, which has psychological stiffness from 9 to 20 kPa^{2,3}. Hard gels with stiffness $50.68 (\pm 0.92)$ kPa were used to mimic cartilage^{2,4,5}. Also, since most *in vitro* work in research labs is carried on polystyrene culture dishes (elastic modulus of polystyrene: ~ 3 GPa), polystyrene served as the fourth substrate. The beating force of the cardiac cells was quantified using a versatile micro-electromechanical system (MEMS) force sensor and it was found that the force for the cells cultured on stiff polystyrene culture plates ($F = 79.46 \pm 17.20$ nN) was consistently larger than those cultured on soft PA gels ($F = 30.16 \pm 3.83$ nN).

The force that the cardiac cells and their aggregates exert on both the substrate and surrounding fibroblasts during their rhythmic contraction and relaxation are important parameters to characterize for applications in cardiac tissue engineering. Several methods have been developed for quantitative measurement of the force that cells apply on their substrates. Micro-

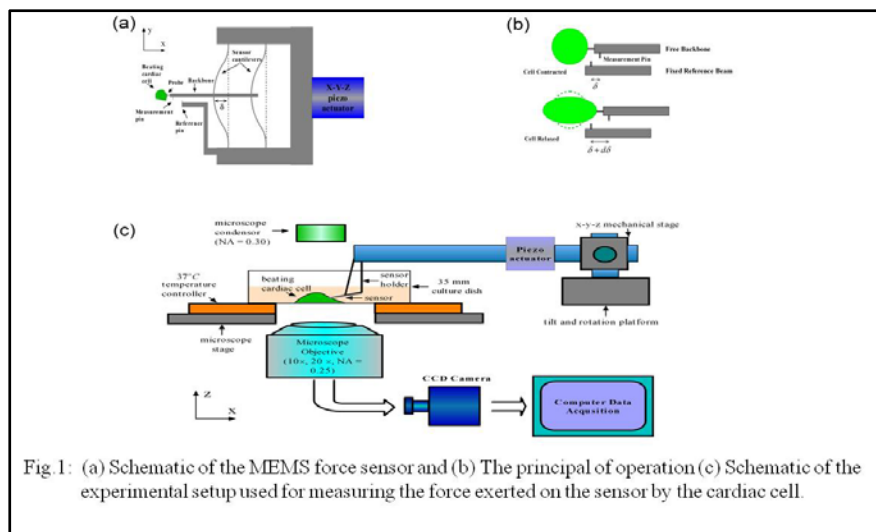
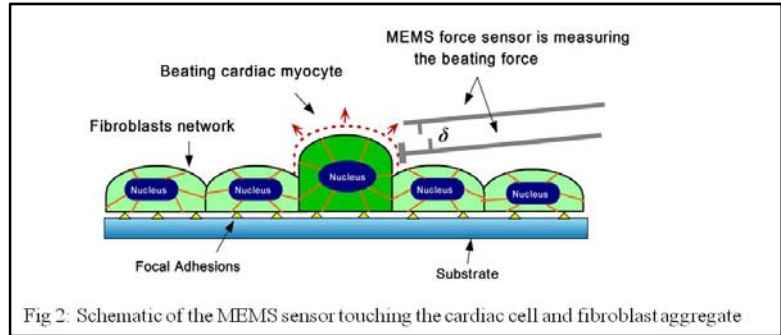


Fig. 1: (a) Schematic of the MEMS force sensor and (b) The principal of operation (c) Schematic of the experimental setup used for measuring the force exerted on the sensor by the cardiac cell.

fabricated silicone elastomeric posts⁶ and fluorescent-beads embedded flexible substrates^{7, 8} are two representative quantitative approaches. However, there is no easy way to determine or estimate the beating force that cardiac cells exert on their surrounding fibroblasts. We characterized the beating force using a novel MEMS-based force sensor.^{9, 10} The schematic of the sensor and its principle of operation are shown in Fig. 1 (a-c). Cells on both polystyrene substrates and 18 kPa gels were characterized at different culture days.

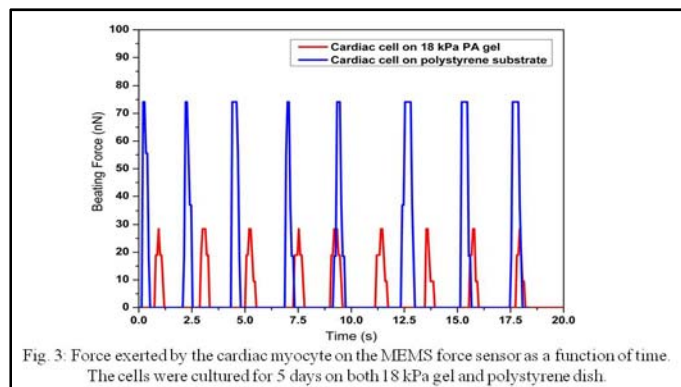


MEMS force sensors were fabricated to measure the force exerted by cardiac cells during their rhythmic contraction and relaxation. The fabrication process and other applications of this MEMS force sensor have been described previously.^{9,10} The effective spring constant of the cantilever beam can be calculated from the dimensions of the cantilever and the material properties of silicon (Si) as shown in Equation 1, or it can be found by atomic force microscopy.

$$k = \frac{32E_{Si}hb^3}{L^3} \quad (1)$$

In equation 1, $E_{Si} = 170$ GPa is the Young's modulus of single-crystal silicon along [110] direction. The width, depth and length of each cantilever beam are $b = 1 \mu\text{m}$, $h = 10 \mu\text{m}$, and $L = 2.5$ mm, respectively. The k is the spring constant of force sensor and is equal to $48.96 \text{ nN } \mu\text{m}^{-1}$. The resolution of the MEMS sensor was about 0.25 nN . The MEMS force sensor was held and driven by the X-Y-Z piezoelectric actuators with 1 nm spatial resolution. The MEMS force has two beams, a fixed (reference) beam and a free (measurement) beam. The sensor touches the cardiac cells membrane along the direction of maximum contraction of the cell. To eliminate the external mechanical indentation, the forward movement of beam is stopped right after it contacts the cell body. The vertical height of sensor is strictly controlled to avoid touching the substrate. Fig. 2 shows the schematic of the MEMS force sensor to measure the force of the cardiac cell.

The force exerted on the MEMS sensor by the cells cultured on polystyrene dish was consistently higher than that by the cells on the soft 18 kPa gel. The duration for one contraction-relaxation cycle on both substrates were found to be 0.6-0.8 seconds. Fig. 3 shows the force as a function of time. Here, we found that the average peak force exerted by the cells on the polystyrene dish shows only 10% variation, from $79.46 \pm 17.20 \text{ nN}$ on the second day to $71.30 \pm 6.38 \text{ nN}$ on the fifth day compared to almost a 50% decrease on the 18 kPa from $67.87 \pm 10.69 \text{ nN}$ on day two to $30.16 \pm 3.83 \text{ nN}$ on day five. There can be various reasons for the larger force on the polystyrene dish as compared to the 18 kPa gel substrate. Firstly, it is well-known that the normal anchorage-dependent cells form irregularly-shaped, highly-dynamic focal adhesions (FAs) on the soft substrates, while the same type of cells



cultured on very rigid substrates, like polystyrene, form stable and well defined focal adhesions.^{11,12} These focal adhesions link the extracellular matrix to intracellular cytoskeleton via the inter-membrane receptors. The focal adhesion points serve as the pivots to assist the intracellular pre-stress build-up and are the sites at which cell traction are transmitted to the substrate. A force balance is established between adhesion and intracellular forces, i.e. pre-stress and beating force. Unstable focal adhesions result in both reduced cell traction between the cardiac cells and the 18 kPa gel, and the less stressed cytoskeleton assembly. To maintain

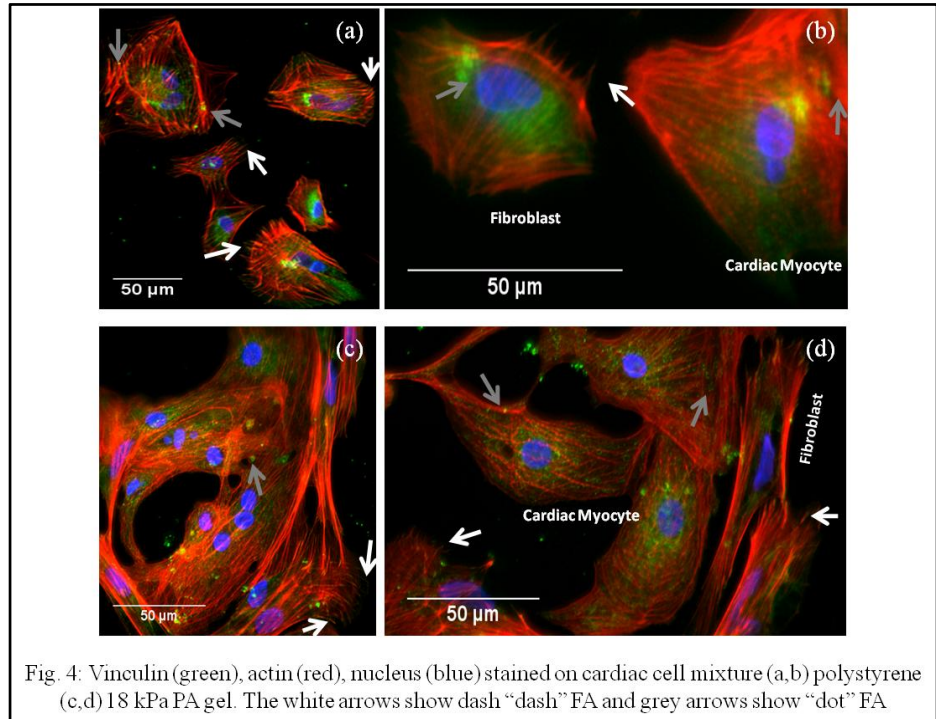


Fig. 4: Vinculin (green), actin (red), nucleus (blue) stained on cardiac cell mixture (a,b) polystyrene (c,d) 18 kPa PA gel. The white arrows show dash “dash” FA and grey arrows show “dot” FA

anchorages with substrate, the beating force cannot exceed the cell traction force. Therefore, cardiac cells cultured on soft substrate down-regulate their beating force to match the weak adhesion force between cells and gel substrate. In contrast, firm focal adhesions between cardiac cells and glass allow cells to apply larger force for rhythmic contraction without breaking the anchorage sites. Secondly, over longer periods of time, cells on soft substrates show reduced expression of actin stress fibers and focal adhesion proteins.^{2,13} The less integrated cytoskeleton leads to further decrease of beating force and force resistance on the 18 kPa gel. Fig. 4 shows the staining of the cardiac cell mixture on the polystyrene (a,b) and the 18 kPa (c,d) substrate. On the both the substrates, the two different types of FA (dot and dash) can be seen. However, on the stiff polystyrene substrate, more number of FA/cell are present compared to the 18 kPa PA gel and hence the cells on the stiff polystyrene substrate exerts a larger force on this substrate.

IV. KEY RESEARCH ACCOMPLISHMENTS

- MEMS force sensors were fabricated to measure the force exerted by cardiac cells during their rhythmic contraction and relaxation.
- Showed that the beating rate of embryonic chicken cardiac myocytes depends on the stiffness of the substrate only during the first few days of culture.

V. REPORTABLE OUTCOMES

VI. CONCLUSION

In summary, we have shown that the beating rate of embryonic chicken cardiac myocytes depends on the stiffness of the substrate only during the first few days of culture. Subsequently, there is a convergence of the beating rate possibly due to mechanical coupling between the cells mediated by the soft substrate or proliferating fibroblasts that bridge between the cells. Our results also show that the beating force by cardiac cells is consistently greater on the rigid polystyrene substrate, most likely because of the formation of very stable focal adhesion complexes compared to few dynamic focal adhesion complexes on soft PA gels. Throughout the five days of culture the beating force and energy that cardiac cells exert on surrounding fibroblast network stay consistent magnitude, which effectively contribute to the beating synchronization over long range. Our cumulative findings can have a significant impact on the design of 3-dimensional cardiac tissue engineered scaffolds.

VII. REFERENCES

1. J. Solon, I. Levental, K. Sengupta, P. C. Georges and P. A. Janmey, *Biophys. J.*, 2007, **93**, 4453-4461.
2. D. E. Discher, P. A. Janmey and Y. L. Wang, *Science*, 2005, **310**, 1139-1143.
3. A. J. Engler, C. C. Krieger, C. P. Johnson, M. Raab, H. Y. Tang, D. W. Speicher, J. W. Sanger, J. M. Sanger and D. E. Discher, *J. Cell Sci.*, 2008, **121**, 3794-3802.
4. A. J. Engler, L. Bacakova, C. Newman, A. Hategan, M. A. Griffin and D. E. Discher, *Biophys. J.*, 2004, **86**, 617-628.
5. A. Gefen and S. S. Margulies, *J. Biomechanics*, 2004, **37**, 1339-1352.
6. J. L. Tan, J. Tien, D. Pirone, D. S. Gray, C. S. Chen, *Proc Nat Acad Eci U.S.A*, 2003, **100**, 1484-1489.
7. Y. L. Yang and R. J. Pelham, *Methods Enzymol.*, 1998, **298**, 489-496.
8. N. Wang, I. Marija, T. Norrelykke, J. Chen, S. M. Mijailovich, J. P. Bulter, J. J. Fredberg, and D. Stamenovi, *Am J Physiol Cell Physiol*, 2002, **282**: C606-C616.
9. S. Yang and M. T. A. Saif, *Rev. Sci. Instrum.*, 2005, **76**, 044301.
10. S. Yang and M. T. A. Saif, *Acta Biomaterialia*, 2007, **3**, 77-87.
11. R. J. Pelham and Y. L. Wang, *Proc. Natl. Acad. Sci. U.S.A*, 1997, **94**, 13661 – 13665.
12. A. J. Engler, L. Bacakova, C. Newman, A. Hategan, M. A. Griffin and D. E. Discher, *Biophys. J.*, 2004, **86**, 617-628.
13. E. Cukierman, R. Pankov, D. R. Stevens and K. M. Yamada, *Science*, 2001, **294**, 1708-1712.

Research Group: Larry Schook

Period Aug'08 to Aug'09

I. Summary of Work

We have successfully mobilized peripheral blood stem cells and collected large numbers of cells via leukapheresis in the pig model. We are continuing work on the characterization portion of year one Milestone 8 “Characterize CD34 expression levels of freshly isolated stem cells from various tissues.” Stem cells from various sources are being characterized for CD34 antigen expression and this task is expected to be completed by February 2010. Concurrently with this task we have begun developing stores of mobilized stem cells as described in year two Milestone 6. We have also initiated training to develop a porcine myocardial infarction model as described in year two Milestone 7.

II. INTRODUCTION

The goals of the Schook subgroup are to generate protein and antibody reagents specifically necessary for the mobilization and characterization of porcine stem cells. These stem cells will be collected and stored for future use in trials of tissue repair following myocardial infarction.

III. BODY

Characterize CD34 expression levels of freshly isolated stem cells from various tissues (First year milestone #8)

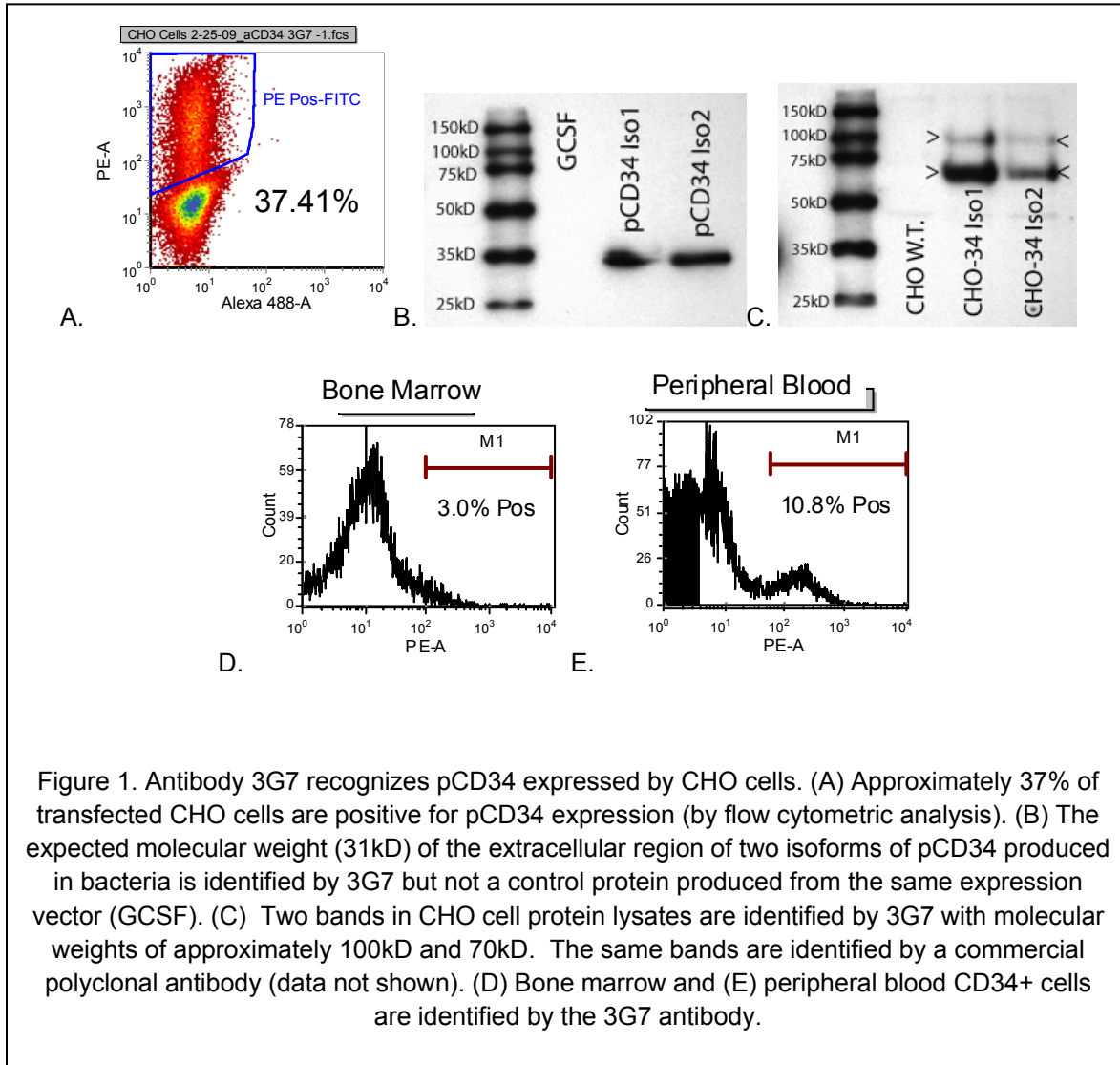
CD34 antibody characterization

Due to the widespread use of the CD34 antigen for the identification of stem cells from both hematopoietic and adipose derived human tissues we have generated monoclonal antibodies to porcine CD34 (pCD34). To date, anti-pCD34 monoclonal antibodies are not commercially available and previous attempts at using antibodies generate to non-porcine CD34 antigens to identify pCD34 have been unsuccessful. A porcine model was selected because of its widespread use as a clinical cardiac model.

We generated a series of monoclonal antibodies to a pCD34 antigen produced in bacteria. One antibody, designated 3G7, was selected for further characterization. We generated a pCD34 expressing CHO cell line (CHO-CD34) and analyzed pCD34 expression by flow cytometry (Figure 1A). To confirm that the antibody is identifying the correct antigen, Western blots were run using both recombinant antigen expressed in bacteria and pCD34 expressed by CHO cells. We have identified two isoforms of pCD34 and have included both

isoforms on the Western blots (Figure 1B and C). The 3G7 antibody recognizes pCD34 antigen expressed in bacteria with the expected molecular weight (31kD) and two bands (~100kD and ~70kD) in CHO cells. A commercial polyclonal antibody (R&D Systems) was used to confirm that the molecular weights of the expressed antigens were the same as those identified by 3G7. Attempts to use the commercial antibody in flow cytometric applications were unsuccessful.

We have isolated adipose derived stem cells (ADSC) from four test animals (tissues taken post-mortem from animals used in IACUC approved protocols). Isolated cells were characterized via flow cytometry using the 3G7 antibody and co-stained with an anti-CD31 antibody (AbD Serotec; FITC conjugated). CD31 (PECAM) is a pan endothelial marker. Since a subset of endothelial cells can be CD34+, dual staining was used to identify non-endothelial CD34+ cells. Freshly isolated cells were 13-70% positive for CD34, similar to values and ranges found for both excised and liposuction derived human cells. Also similar to human cells, porcine ADSC rapidly lose CD34 expression in culture with some samples losing all CD34 expression by day 5 of culture. Subsets of CD34+ and CD34- cells were also plated in colony forming unit-fibroblast (CFU-F) assays to determine the clonogenic/stem cell potential of the two subsets. Cells in the CD34+ subset exhibit a colony forming rate 3-7 times higher than the CD34- subset.



Both bone marrow aspirates and peripheral blood have also been characterized by flow cytometry using the 3G7 antibody in animals approximately 4 months old (Figure 1D and E). The percentage of CD34+ cells measured in the bone marrow (3.0%) was in the expected range of 1-5%. The number of CD34+ cells in the peripheral blood (<10%) is much higher than expected. While circulating CD34+ endothelial progenitor cells (EPCs) and CD34+ hematopoietic stem cells occur at higher percentages in younger animals, we will explore the possibility that the 3G7 antibody is cross reacting with a secondary antigen expressed by peripheral blood cells using Western Blot analysis.

Leukapheresis in the pig model

We have established a porcine model of stem cell mobilization to the peripheral blood mirroring protocols used for human stem cell mobilization. This procedure involves the

administration of the growth factor granulocyte colony stimulating factor (GCSF) over a period of four days with collection of peripheral white blood cells on the final day. To perform these experiments we have produced recombinant porcine GCSF (pGCSF) in bacteria and have confirmed by limulus testing that the product has less than 0.5 endotoxin units (EU) per microgram of protein. This level of EU is below the recommended FDA limit for the dose of 10 $\mu\text{g}/\text{kg}$ GCSF.

In order to emulate existing technologies for the collection of large numbers of bone marrow derived stem cells, we have purchased a COBE spectra leukapheresis system and have received training on its operation. We have performed stem cell mobilizations using recombinant porcine GCSF produced on our laboratory and carried out leukapheresis collections on 4 test animals. Total collection time (4-5 hours), sample volume collected (240-300mL), and total white blood cells collected ($50\text{-}80 \times 10^9$) are all similar to values during clinical human leukapheresis. We have confirmed that machine collection settings based on colorimetric hematocrit percentage are similar to clinical settings. Blood cell differential characterization of products collected at different machine settings is ongoing.

Develop porcine myocardial infarction model (Second year milestone #7)

We have received training from Dr. Michael Swindle, D.V.M., in the techniques necessary to place cardiac catheters for a myocardial infarction model. The training occurred July 27-29 and covered general techniques, laboratory and surgery set-up, and cardiac catheter placement. During that training we successfully placed catheters in both the Left Anterior Descending (LAD) and Circumflex arteries. A chart correlating left anterior descending (LAD) artery occlusion with extent of infarcted tissue will be generated. This information will be used to reliably produce similar injury in multiple animals which can be treated with various stem cell and/or material therapies.

IV. KEY RESEARCH ACCOMPLISHMENTS

- Produced and characterized anti-porcine CD34 antibody which will be used to isolate CD34 + stem cells from the leukapheresis collections
- Received training to establish the porcine myocardial infarction model
- Optimized porcine stem cell mobilization and collection of these mobilized cells via leukapheresis
- Mobilized and stored peripheral blood stem cells in both blood bags (20mL) and smaller analytical aliquots (1.8 and 4mL) from two test animals ($>100 \times 10^9$ total cells)

V. REPORTABLE OUTCOMES

- Publication in preparation: Jensen TW, Swanson DA, Rund LA, and Schook LB. An anti-porcine CD34 antibody recognizes multiple isoforms of porcine CD34.

- Publication in preparation: Jensen TW, Rund LA, Clark S, Smith S, and Schook LB. Methods for COBE Spectra leukapheresis in the pig.
- Publication in preparation: Jensen TW, Swanson DA, Rund LA, and Schook LB. CD34+ cells in the peripheral blood of pigs.
- American Heart Association Grant application: Alginate Encapsulated Adipose Derived Stem Cells for Myocardial Infarction Repair. Jensen TW
- NIH R21 Grant application: Controllable in vitro platforms that mimic key aspects of myocardial infarction. Schook LB and Timp G.
- Developed anti-porcine CD34 monoclonal antibody
- Developed porcine stem cell mobilization model
- Mobilized porcine peripheral blood stem cell bank started

VI. CONCLUSION

We have created and characterized an anti-porcine CD34 antibody capable of recognizing the antigen in both flow cytometry and Western Blot applications. The CD34 antigen is important in stem cell research due to its widespread use in identifying stem cell subsets in a variety of tissues. It is of particular interest in several current clinical trials exploring the use of CD34+ cell subsets for therapies following myocardial infarction. The importance of this reagent in the pig model is the widespread use of swine for cardiac research. This large animal preclinical model provides a more substantive measure of a variety of cardiac therapies than smaller rat or murine models. Characterization of CD34+ cells in the pig model will increase its utility for cardiac research. We have also begun the development of a porcine myocardial infarction model. This work will provide a large animal model of cardiac damage to explore application of cell-based therapies.

Research Group: **Hyun Joon Kong research group**

Period Aug'08 to Aug'09

I. Summary of Work

Kong's group's goal is to design a cell encapsulating hydrogel which can be readily integrated with a stereolithographic apparatus (SLA) and also presents chemical and mechanical properties proper to support cellular viability, growth, differentiation and growth factor secretion. During the first year, Kong group focused on developing a method to independently control mechanical properties, swelling ratio and degradation rate of a hydrogel. First, Kong's group has synthesized the biodegradable methacrylic alginate (MA) and used it to control the elastic modulus and degradation rate in an independent manner. The hydrogel cross-linked with hydrolytically labile oxidized methacrylic alginate was used as a VEGF-releasing device, which stimulated the capillary blood vessel growth. Second, Kong's group further combined the MA and PEG diacrylates (PEGDA) to control the hydrogel stiffness and swelling ratio in an independent manner. The MA and PEGDA hydrogel is now being combined with the SLA unit to assemble the vascularized 3D tissue

engineering scaffold, which is expected to improve the cell viability and functions in a 3D matrix. The results of our study will be an invaluable paradigm of a 3D cell encapsulation device prepared with a broad array of gel-forming polymers. This study will also greatly expedite the use of hydrogels as a 3D cell encapsulation device in both biology and clinical settings.

II. INTRODUCTION:

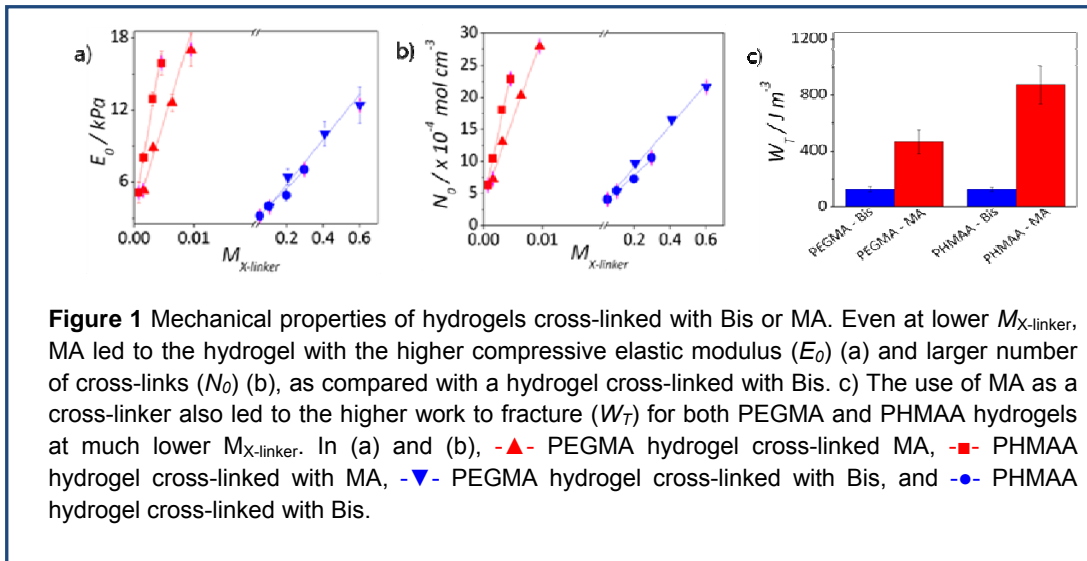
The goal of our research was to develop an advanced cell-encapsulating hydrogel which can support cell viability and function to recreate a cardiac muscle tissue using tissue engineering technology⁽¹⁾. Specifically, we had focused on achieving two sub-goals; 1) Develop methods to decouple the dependency of hydrogel mechanics on the degradation rate and the dependency of hydrogel mechanics on the swelling ratio, so we could control the gel stiffness without significantly altering hydrogel degradation rate and permeability⁽²⁾, and 2) Develop a cell-encapsulating vascularized bioactive hydrogel, so we could enhance the cellular viability and diverse activities including growth, differentiation and growth factor secretion⁽³⁾.

III. BODY:

A. Independent control of mechanical properties of hydrogel

A.1. Synthesis of OMA and characterization of a hydrogel cross-linked by OMA

The OMA was prepared sequentially by i) irradiation of alginate with γ -rays to reduce its molecular weight⁽⁴⁾, ii) an oxidation reaction of the alginate, and iii) a chemical reaction to link methacrylic groups to the oxidized alginate. Effects of cross-linkers on the stiffness and toughness of both PEGMA and PHMAA hydrogels were examined. The hydrogel stiffness quantified with an elastic-modulus measurement was significantly dependent on both $M_{X-linker}$ (molar ratio of methacrylates between the cross-linker and PEGMA or PHMAA) and the chemical structure of the cross-linker (Fig 1 (a)). Interestingly, the hydrogels cross-linked with MA were stiffer than those cross-linked with Bis (conventional short cross-linker), even at much lower $M_{X-linker}$ (Fig. 1(a)). Despite the higher stiffness, the hydrogel cross-linked with MA also presented a greater resistance to fracture than the hydrogel cross-linked with Bis by one order of magnitude (Fig. 1(c)). Independent control of hydrogel stiffness and toughness could be achieved with the greater valency of methacrylic groups and longer chain length of MA than Bis.



A.2. Controlling in vivo angiogenesis using growth factor encapsulated by hydrogels

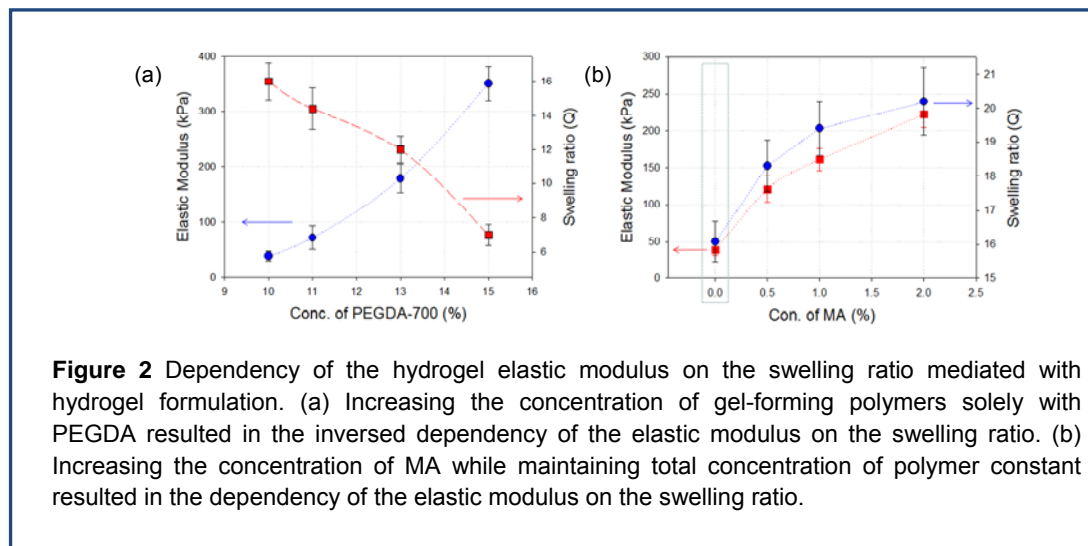
The role of OMA in regulating hydrogel function to release angiogenic growth factors and subsequently promote the neovascularization in a connective tissue was evaluated. The vascular endothelial growth factor (VEGF) was encapsulated in PEGMA hydrogels cross-linked with Bis or OMA, and the VEGF-hydrogel construct was implanted on the chorioallantoic membrane (CAM) of chick embryos. The implanted gel was gradually incorporated into the CAM within a day. Hydrogels incorporated into the CAM did not trigger any severe host inflammatory response as compared with a control tissue onto which no hydrogel was implanted. The implantation of hydrogel containing VEGF resulted in an increase in the number of mature blood vessels marked with α -smooth muscle actin antibody. The hydrogel cross-linked with OMAs further increased the density of mature blood vessels, 1.5 times more than that cross-linked with Bis.

B. *In situ* cell encapsulation into a vascularized bioactive hydrogel using a SLA

B.1. Control of nano-sized pores using PEGDA and MA

We hypothesized that the diameter of nano-sized pores would be increased with mass fraction of MA, because charged units and multivalent hydroxyl groups of alginate increase the hydrogel pore size and subsequent permeability. This hypothesis was examined using a composite hydrogel consisting of PEG diacrylates (PEGDA) and MA. Increasing the polymer concentration of the hydrogel solely with PEGDA resulted in the inverted dependency of the elastic modulus on the swelling ratio, as expected (Fig. 2(a)). Interestingly, incorporation of methacrylic alginate significantly increased both elastic modulus and swelling ratio of pure PEGDA hydrogel by one order of magnitude (Fig. 2(b)).

The hydrogel consisted of PEGDA and MA, so the hydrogel diameter of nano-sized pore could be controlled in a desire manner.



B.2. Control of micro-sized pores using a stereolithographic apparatus (SLA)

The hydrogel formulation was tested for the assembly of a microporous 3D scaffold using the 3D stereolithographic apparatus (SLA). Specifically, we hypothesized that incorporating interconnected micro-sized pores into a cell-encapsulating hydrogel would significantly improve the cell viability, depending on the spacing between micro-sized pores. Our hypothesis was examined by combining a hydrogel formulation to control the diameter of the nano-sized pores over a broad range with a SLA to control micro-sized pores. The SLA is a light-mediated rapid prototyping system that builds 3D objects in sequential layer-by-layer steps from a computer-aided 3D image ⁽⁵⁾. The role of micro-sized pore and spacing between them by combining a hydrogel formulation in enhancing cell-viability and regulating cell-functions is currently being investigated.

IV. KEY RESEARCH ACCOMPLISHMENTS:

- Synthesize bioactive, bio-degradable methacrylic alginate (MA) and demonstrate hydrogel fabrication with stereo-lithographic apparatus: Kong's group has synthesized the biodegradable methacrylic alginate and used it to control the elastic modulus and degradation rate an independent manner. The hydrogel was successfully used as a VEGF-releasing device which stimulated the capillary blood vessel growth. Kong's group further combined the methacrylic alginate and PEG diacrylates to control the hydrogel stiffness and swelling ratio in an independent manner. The hydrogel formulated with the effort showed enhanced cell viability. Besides, the gel is being integrated with the SLA unit to assemble the vascularized 3D tissue engineering scaffold.

- Functionalize the surface with fibronectin, laminin, collagen, and characterize their density: Kong's group has recently modified cell adhesion proteins with methacrylic groups and successfully linked them to the hydrogel-forming methacrylic alginate. Kong's group has also labeled the cell adhesion proteins with flurophores to quantitatively evaluate the density of cell adhesion molecules in the 3D gel matrix.

V. REPORTABLE OUTCOMES:

- List of papers published in peer-reviewed Journals
 - 1) Cha, C., Kohman, R. and Kong, H.J., Biodegradable polymer crosslinker: Independent control of stiffness, toughness, and hydrogel degradation rate. *Advanced Functional Materials* (2009) 19, 1-7
- List of abstracts and presentations in related conferences
 - 1) Cha, C. and Kong, H.J., Biodegradable polymeric crosslinker: Independent control of mechanics and degradation. Oral presentation at *American Chemical Society National Fall Meeting*, Washington D.C (August 2009)
 - 2) Jeong, J.H., Chan V., Cha. C., Bashir. R., and Kong, H.J., In situ cell encapsulation into a vascularized hydrogel matrix using stereolithography. Accepted for the poster presentation at *Biomedical Engineering Society National Fall Meeting*, Pittsburgh (October 2009)
 - 3) Jeong, J.H., Chan V., Cha. C., Bashir. R., and Kong, H.J., In situ cell encapsulation into a vascularized hydrogel matrix using stereolithography. Accepted for the oral presentation at *America Institute of Chemical Engineers Annual Meeting*, Nashville (November 2009).

VI. CONCLUSION: The incorporation of oxidized methacrylic alginate into a poly(ethylene glycol) hydrogel allowed us to control the mechanical properties, swelling ratio and degradation rates in an independent manner. The independent control of mechanical properties and degradation rates of a hydrogel enabled the refined control of angiogenic growth factor release and subsequently improve the capillary blood vessel formation. The independent control of mechanical properties and swelling ratio also enabled us to incorporate cells into a stiff hydrogel and also to improve the cell viability and activity to secrete angiogenic growth factors. Overall, the oxidized methacrylic alginate developed in this project will be broadly useful to regulating

VII. REFERENCES:

- (1) Lee K.Y., and Mooney D.J., *Chem. Rev.* 2001, 101, 1869 (2) Kong H.J., Wong E., and Mooney D.J., *Biomacromolecules* 2003, 36, 4582 Fischbach, C., Kong H.J., Hsiong S., Evangelista M., Yuen W., and Mooney D.J., *PNAS (USA)* 2009, 106, 399 (4) Kong H.J., Smith M.K., and Mooney D.J., *Biomaterials* 2003, 24, 4023 (5) Karina A., Brenda K., and Wicker R.B., *Annals of Biomedical Eng.* 2006, 34, 1429

Research Group: Brian Cunningham

Period Aug'08 to Aug'09

Annual Report from Project Subgroups

- I. **Summary of Work** Development of label-free imaging of cell adhesion to surfaces using Distributed Feedback Laser Biosensor (DFBLB) surfaces and related detection instruments.

- II. **INTRODUCTION:** Our aim is to develop a high sensitivity and high spatial resolution method for measuring cell adhesion, proliferation, and chemotaxis upon a surface. Using a distributed feedback optically pumped laser that is fabricated upon plastic surfaces by replica molding, we demonstrate high resolution label-free detection of adsorbed biomolecules and cells. The biosensor surface can be prepared with hydrogels that are being considered for the 3D cell scaffold, and used as a tool for evaluating the attachment, growth, and differentiation of cells.

III. BODY

DFBLB Operation and Device Structure

The DFB laser biosensor is classified as active optical resonator. Active optical resonators can produce their own narrow bandwidth light, provide high Q factor with simple coupling to the excitation source and collection optics for detecting small changes in wavelength, while retaining excellent sensitivity, as defined by the magnitude of the wavelength shift. For a DFB laser, the emission wavelength is determined by the Bragg condition: $m\lambda = n_{\text{eff}}\Lambda$, where m is the diffraction order, Λ denotes the grating period, and n_{eff} represents the effective refractive index that depends on the optical indices of the corrugated waveguide, the surrounding material and strength of electric field in each material. The interaction between biomaterial immobilized on the sensor surface and the evanescent field will result in the redistribution of the electric field in the resonant cavity and modify the n_{eff} . According to the Bragg condition, the change of n_{eff} will introduce a corresponding shift of the laser wavelength, which is continuously monitored. In this work, we make use of a second-order Bragg grating that supports a vertical emission mode by first-order diffraction, resulting in a simple pumping and detection setup.

The DFB laser consists of three layers: the low index grating substrate that serves as the cladding layer; the laser dye doped high index organic gain film that provides light confinement, feedback and amplification; another high refractive index layer on the top of the laser cavity to promote the bimolecular immobilization and enhance the sensor sensitivity.

A cross-sectional diagram (not to scale) of the DFB laser biosensor structure is shown in Fig. 1. The replicated gratings have a period, depth, and RI of 400 nm, 40 nm, and 1.38, respectively. The grating structures can be uniformly fabricated inexpensively over large surface areas using

nanoreplica molding technique. The waveguide layer, i.e., gain medium, was fabricated by spin-coating Rhodamine 590 doped SU-8 onto grating surface. The titanium dioxide thin film was deposited on top of the DFB laser surface by e-beam evaporation.

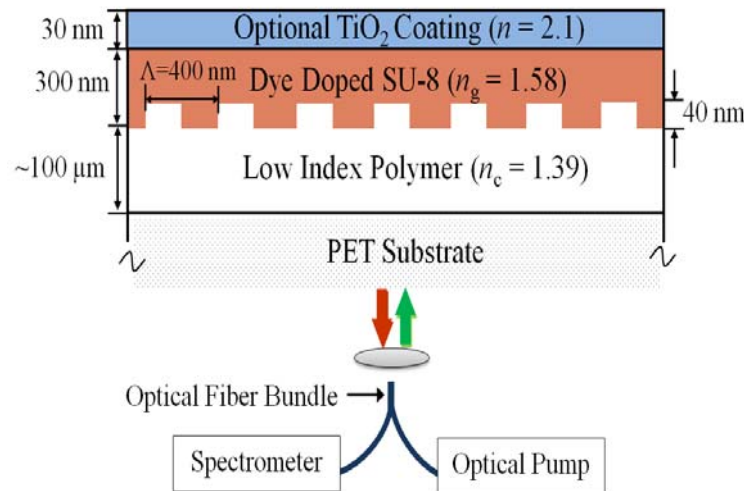


Figure 1. Cross Sectional schematic diagram of the DFBLB

Detection Instrument

A schematic of the biosensor detection instrument is shown in Fig.2. An Nd: YAG laser illuminates the laser sensor at normal incidence with 10 nsec pulses of $\lambda = 532$ nm wavelength. The function of the beam expander is to minimize the exciting spot size. The pump light is expanded and focused onto the sensor through a 20x microscope objective placed beneath the sensor. The laser emission is collected with an optical fiber (diameter=0.4 mm) and delivered to a CCD-based spectrometer with 0.0165 nm resolution (Horiba Jobin Yvon iHR550). The Peak Wavelength Value (PWV) of laser emission is determined by fitting the laser spectrum to a Lorentzian function.

To achieve kinetic PWV detection and spatial PWV imaging, a software experimental management system was developed. For kinetic measurements, the pumping position is fixed and the laser emission wavelength is continuously measured. When working in imaging mode, a motorized stage will translate the sensor in the plane perpendicular to the pumping light to get the spatial distribution of peak wavelength values. The spatial resolution is determined by the step size of the motor stage, the exciting spot size and the traveling distance of the feedback light. For a typical experiment, we need to scan the sensor twice, before and after the bimolecular binding, to determine the PWV shift.

The device chip is integrated into standard 96-well microplates to facilitate the detection. In order to get the spatial PWV image, we scanned 75 spots with 400 microns spacing both in X and Y direction within one well. Moreover, an algorithm was developed and implemented to select peaks that have both high enough intensity and narrow enough linewidth (< 0.1 nm). This can guarantee more precise and reliable measuring results.

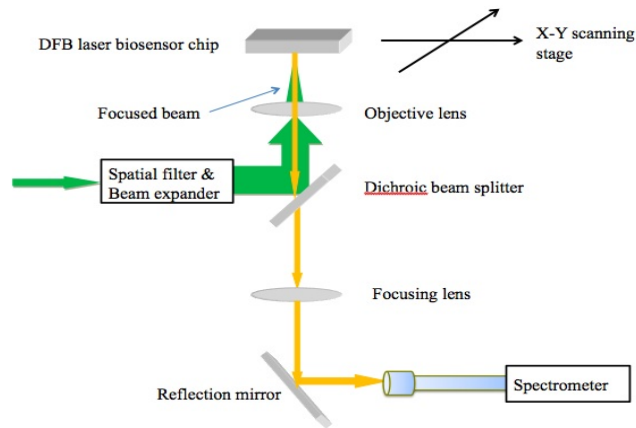


Figure 2 Schematic diagram of detection instrument for the DFBLB

DFBLB Measurements

A dielectric nanorod structure is used to enhance the label-free detection sensitivity of the DFBLB. The device is comprised of a replica molded plastic grating that is subsequently coated with a dye-doped polymer layer and a TiO₂ nanorod layer produce by the glancing angle deposition technique. The DFBLB emission wavelength is modulated by the adsorption of biomolecules, whose greater dielectric permittivity with respect to the surrounding water media will increase the laser wavelength in proportion to the density of surface-adsorbed biomaterial. The nanorod layer provides greater surface area than a solid dielectric thin film, resulting in the ability to incorporate a greater number of molecules. The detection of a monolayer of the protein polymer poly (Lys, Phe) is used to demonstrate that a 90 nm TiO₂ nanorod structure improves the detection sensitivity by a factor of 6.6x compared to an identical sensor with a nonporous TiO₂ surface.

The detected single mode DFBLB emission spectrum is shown in Figure 3. The measured spectrum is fitted with a Lorentzian distribution model using MATLAB to precisely determine the peak wavelength value (PWV) of laser emission. The observed lasing wavelength is $\lambda = 597.045$ nm when the sensor surface is immersed in water. Lasing occurs at the one band edge near the Bragg resonance, determined by the equation $m\lambda_{Bragg} = 2n_{eff}\Lambda$, where $m = 2$ is the order of diffraction, n_{eff} is the effective refractive index of the resonant mode, and Λ is the grating period. As shown in Figure ??, an emission linewidth (full-width a half-maximum) of $\Delta\lambda = 0.0375$ nm is obtained, corresponding to a Q factor of 15,000.

Figure 3 shows the laser emission spectrum of a DFBLB with a $t=67$ nm nanorod coating. The left inset of Figure 3 shows the dependence of the laser emission wavelength as a function of nanorod thickness with the DFBLB surface immersed in DI water. The TiO₂ nanorod layer causes the PWV to shift to longer wavelength. Meanwhile the linewidth of the emission spectrum remains as narrow as the DFB structure without a nanorod TiO₂ film coating.

To demonstrate the sensitivity enhancement resulting from the TiO₂ nanorod layer, sensitivity to surface mass adsorption was characterized. Sensors with either a 30 nm solid

TiO₂ film or nanorod TiO₂ films of 22nm, 30 nm, 67 nm, 90 nm were prepared. All the sensors were coated with a single monolayer of protein using the following protocol. First, the sensors were exposed to a phosphate buffered saline (PBS) solution for 15 min, after which a baseline PWV measurement was taken from each biosensor microplate well, as described above. Next, the PBS solution was removed by pipette and the wells were refilled with 1 mg/ml solution of the protein polymer poly (Lys, Phe) (PPL) (Sigma–Aldrich). In previous research, PPL has been demonstrated to form a self-limiting single monolayer coating upon dielectric surfaces (REFERENCE). Previous characterization of PPL films estimates that the film thickness is ~15 nm with a refractive index of n~1.45. The PPL solution was incubated with the sensor surfaces for 1 hr, after which the PPL solution was removed and the sensor surface was rinsed with PBS solution 3 times to remove any PPL that was not firmly attached to the sensor surface. With PBS solution in the biosensor microplate wells, a second set of PWV measurements were gathered. The baseline PWV measurements were subtracted on a well-by-well basis to determine the PWV shift for each sensor, shown in Figure 3.

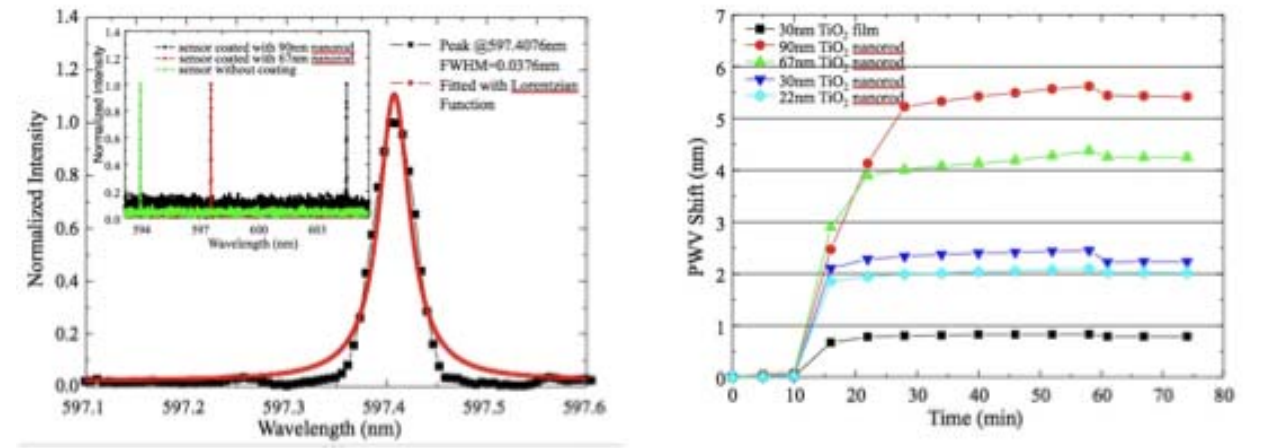


Figure 3. Output spectra from the DFBLB and laser output wavelength as a function of time for adsorption of a protein monolayer to sensors prepared with nanoporous coatings of titanium oxide.

Label-Free Cell Images

Concurrently, a label-free imaging microscope has recently been demonstrated for the

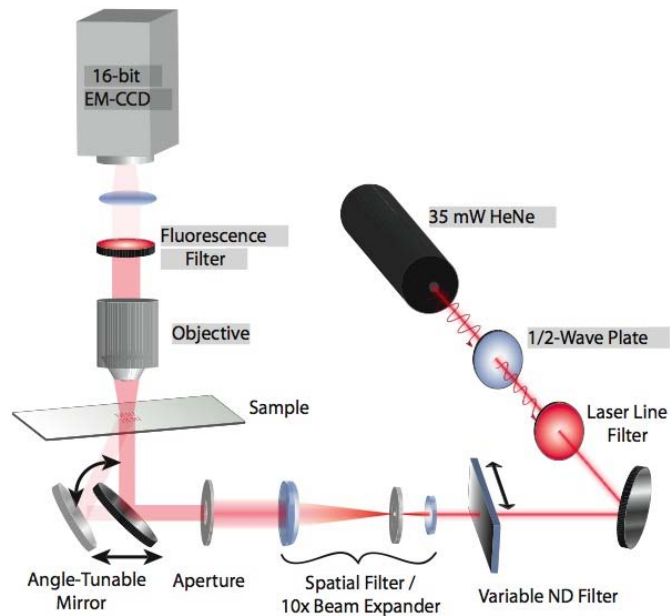


Figure 4. Label-free imaging instrument for measuring cell surface attachment to biosensor surfaces.

first time using Photonic Crystal (PC) biosensor surface structures with ~ 1 micron pixel resolution. A schematic drawing of the label-free microscope is shown in Figure 4, and an image of several surface-adsorbed pancreatic cancer cells is shown in Figure 5. The system utilizes a PC surface that reflects collimated light from a monochromatic light source (a 633 nm HeNe laser) at only one particular angle. Scanning the angle of a mirror beneath the PC through a series of small angle increments while measuring the transmitted light intensity with a CCD camera enables determination of the Angle of Minimum Transmission (AMT), where the AMT shifts to lower angles due to the adsorption of biomolecules or cells. We are currently determining the spatial resolution limits of this imaging technique, and have begun experiments to demonstrate label-free detection of pancreatic cancer cells. It will be our goal to image adsorption of cardiac cells on the PC surface when the cells are available.

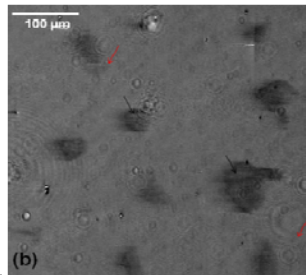


Figure 4 Label-free images of surface adsorbed pancreatic cancer cells on a biosensor surface. Dark regions represent pixels with greater PWV due to the refractive index of the attached cells with respect to the surrounding media.

V. KEY RESEARCH ACCOMPLISHMENTS:

- Demonstration of DFB laser biosensor and detection of adsorbed protein layers.
- Design and assembly of DFBLB detection instrument, including software to gather label-free images.
- Development of a fabrication process for producing DFBLB surfaces and attachment into microplates.
- Detection of label-free images of attached cells.

VI. REPORTABLE OUTCOMES:

- Manuscript for Applied Physics Letters describing the DFBLB enhanced sensitivity using dielectric nanorod surfaces (in preparation).
- Our goal is to prepare a high-impact journal article (Science or Nature Photonics) on the DFBLB imaging capability and its applications to microarray and cell imaging. However, a more thorough set of experimental results must be gathered,

VII. CONCLUSION: We have shown, for the first time, a DFBLB sensor and detection instrument with capability for imaging the adsorption of biomaterial on a surface in a label-free fashion. Initial images had a pixel resolution of ~12 microns, but recent improvements in the optics and positioning stage will enable ~1 micron pixel resolution. This pixel resolution will enable monitoring the attachment of cells to a variety of hydrogel and extracellular matrix surfaces. We have also demonstrated a separate label-free biosensor imaging method based upon photonic crystal surfaces, and used the system to obtain label-free images of pancreatic cancer cells. The photonic crystal biosensor imaging approach will have the same sensitivity as the DFBLB, but sensitivity and spatial resolution appear to be good enough for monitoring cells. The photonic crystal sensors currently have more uniform performance over large surface areas than the DFBLB, which has thus far facilitated imaging. In the next quarter, we plan to image cardiac myocytes and stem cells on the photonic crystal biosensor and upon the DFBLB surface.

Appendix: Publications

Biodegradable Polymer Crosslinker: Independent Control of Stiffness, Toughness, and Hydrogel Degradation Rate

By Chaenyung Cha,* Richie E. Kohman, and Hyunjoon Kong*

Hydrogels are being increasingly studied for use in various biomedical applications including drug delivery and tissue engineering. The successful use of a hydrogel in these applications greatly relies on a refined control of the mechanical properties including stiffness, toughness, and the degradation rate. However, it is still challenging to control the hydrogel properties in an independent manner due to the interdependency between hydrogel properties. Here it is hypothesized that a biodegradable polymeric crosslinker would allow for decoupling of the dependency between the properties of various hydrogel materials. This hypothesis is examined using oxidized methacrylic alginate (OMA). The OMA is synthesized by partially oxidizing alginate to generate hydrolytically labile units and conjugating methacrylic groups. It is used to crosslink poly(ethylene glycol) methacrylate and poly(*N*-hydroxymethyl acrylamide) to form three-dimensional hydrogel systems. OMA significantly improves rigidity and toughness of both hydrogels as compared with a small molecule crosslinker, and also controls the degradation rate of hydrogels depending on the oxidation degree, without altering their initial mechanical properties. The protein-release rate from a hydrogel and subsequent angiogenesis *in vivo* are thus regulated with the chemical structure of OMA. Overall, the results of this study suggests that the use of OMA as a crosslinker will allow the implantation of a hydrogel in tissue subject to an external mechanical loading with a desired protein-release profile. The OMA synthesized in this study will be, therefore, highly useful to independently control the mechanical properties and degradation rate of a wide array of hydrogels.

1. Introduction

Hydrogels are increasingly used for various biological applications including drug delivery, cell culture/transplantation, and tissue

engineering.^[1–3] The successful use of hydrogels in these applications greatly relies on their physical and chemical properties including mechanical rigidity, resistance to fracture, degradation rate, and interaction with bioactive molecules and cells.^[1] Controlling these properties in a desired manner is still a significant challenge in hydrogel design, because of their interdependency. For example, a hydrogel should be rigid enough to maintain its structural integrity for a sufficient period of time to hold drug molecules and cells loaded in the matrix.^[1,2] However, increasing the gel stiffness results in a brittle gel, which is readily fractured at small deformations.^[1,4–6] Certain applications require hydrogels to be biodegradable, but the hydrogel degradation rate is dependent on the hydrogel stiffness.^[1,7]

Extensive efforts have been made to control the mechanical properties of hydrogels over a broad range and subsequently create a rigid and tough hydrogel. Good examples include a double-network hydrogel, a hydrogel containing freely movable crosslinks, a clay-filled hydrogel and an ionically crosslinked hydrogel.^[8a–c,21] Separately, there have been some efforts to decouple the dependency of hydrogel stiffness and degradation rate via chemical

modification of ionically crosslinkable polysaccharide.^[11b,13] However, it is still challenging for the currently available hydrogels to control stiffness, toughness and degradation rate in an independent manner.

It is commonly known that the chemical structure of a crosslinker plays a critical role in controlling the physical properties of a hydrogel. Therefore, we hypothesized that a polymer which presents multi-methacrylic groups and possesses hydrolytically labile units would radically crosslink a broad array of polymers to form a hydrogel and also tune its mechanical properties and degradation rate.^[9a,b] This hypothesis was examined with oxidized methacrylic alginate (OMA) as a model biodegradable polymer crosslinker. The OMA was synthesized by modifying alginate to be hydrolytically labile and also to react with any methacrylic gel-forming polymer.^[10a–c] The function of OMA in modulating hydrogel properties and degradation rate was

[*] C. Cha, R. E. Kohman
Department of Chemistry
University of Illinois, Urbana-Champaign
Urbana, IL 61801 (USA)
E-mail: ccha2@illinois.edu

Prof. H. Kong
Department of Chemical and Biomolecular Engineering
University of Illinois, Urbana-Champaign
Urbana, IL 61801 (USA)
E-mail: hjkong06@illinois.edu

DOI: 10.1002/adfm.200900865

examined with poly(ethylene glycol) methacrylate (PEGMA) and poly(*N*-hydroxymethyl acrylamide) (PHMAA) hydrogels, both of which were crosslinked with OMA. The hydrogel crosslinked with OMA was further tested as a drug-delivery vehicle to release proteins in a sustained manner and subsequently stimulate vascular network formation in vivo.

2. Results

2.1. Synthesis of OMA

The OMA was prepared sequentially by i) irradiation of alginate with γ -rays to reduce its molecular weight, ii) an oxidation reaction of the alginate, and iii) a chemical reaction to link methacrylic groups to the oxidized alginate (Fig. 1a). The irradiation significantly reduced molecular weight from 250 000 to 100 000 g mol⁻¹, as previously reported.^[10a] The oxidation reaction opened an alginate sugar ring to introduce hydrolyzable acetal-like linkages in polymer chains, as confirmed by spectroscopic analysis using ¹H-NMR (Fig. S1, Supporting Information).^[11,12] The oxidation of irradiated alginate slightly decreased the molecular weight to the same order as previously reported.^[11b]

The chemical reaction between oxidized alginate and 2-aminoethyl methacrylate resulted in oxidized alginate presenting methacrylic groups (OMA), as confirmed with ¹H-NMR analysis (Fig. S1, Supporting Information).^[10b,c] The proton peaks of OMA were broader than those in unreacted 2-aminoethyl methacrylate (NH₂-MA), which showed very sharp peaks.

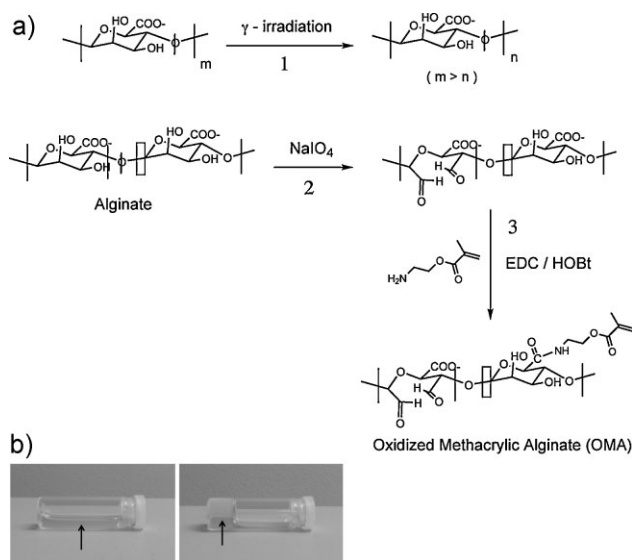


Figure 1. a) Synthesis of oxidized methacrylic alginate (OMA). Alginate was first irradiated with γ -rays (1) and subsequently oxidized with NaIO₄ to introduce a hydrolytically labile acetal-like unit (2). Finally oxidized alginate was chemically linked with 2-aminoethyl methacrylate using aqueous EDC chemistry (3). b) At $M_{X-linker}$ of 0.01, the mixture of PEGMA and Bis kept a liquid state (left photo), while the mixture of PEGMA and methacrylic alginate (MA) resulted in the hydrogel (right photo). The mixture of PEGMA and crosslinker is identified with an arrow.

Furthermore, all the peaks were slightly shifted from their positions. The shifted NMR peaks indicated that the movement of NH₂-MA was restricted by the chemical attachment to the highly viscous alginate chains, which could not be seen in free NH₂-MA. In this study, the number of methacrylates linked to a single alginate was kept constant at 120, and the number of oxidized uronic acid residues per polymer chain was varied from 25 to 50.

2.2. Decoupled Control of Stiffness and Toughness of Hydrogels Using Methacrylic Alginate (MA)

Effects of crosslinkers on the stiffness and toughness of both PEGMA and PHMAA hydrogels were examined. In this study, the non-oxidized methacrylic alginate (MA) or *N,N'*-methylenebis-acrylamide (Bis) was used as a crosslinker. The molar ratio of methacrylates between the crosslinker and PEGMA or HMAA ($M_{X-linker}$) was changed to control hydrogel properties. With the use of Bis as a crosslinker, both PEGMA and PHMAA hydrogels were formed with $M_{X-linker}$ larger than 0.10. In contrast, the use of OMA as a crosslinker significantly decreased the critical $M_{X-linker}$, the lowest $M_{X-linker}$ to form a hydrogel, by one order of magnitude (Fig. 2a and b). Within the concentration range of OMA used to prepare the PEGMA or PHMAA hydrogel, the OMAs alone could not form a hydrogel. Conversely, without Bis or OMA, neither the PEGMA or PHMAA was able to form the hydrogel via radical crosslinking.

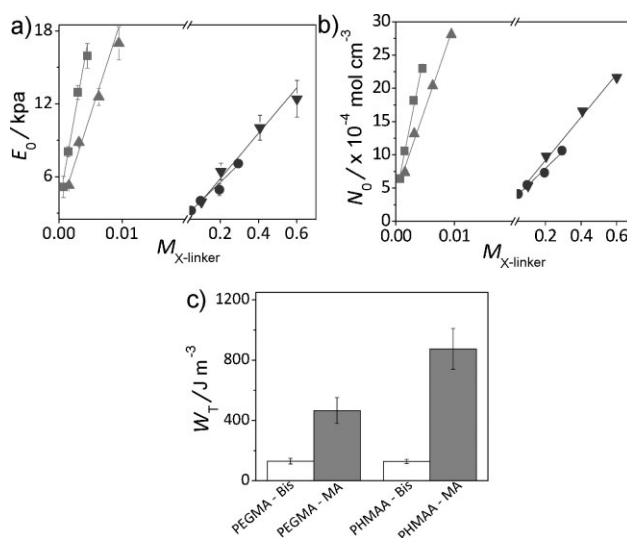


Figure 2. Mechanical properties of hydrogels crosslinked with Bis or MA. Even at lower $M_{X-linker}$, MA led to a hydrogel with a higher compressive elastic modulus (E_0) (a) and larger number of crosslinks (N_0) (b), as compared with a hydrogel crosslinked with Bis. c) The use of MA as a crosslinker also led to the higher work to fracture (W_f) for both PEGMA and PHMAA hydrogels at much lower $M_{X-linker}$. In (a) and (b), -▲- represents PEGMA hydrogel crosslinked with MA, -■- represents PHMAA hydrogel crosslinked with MA, -▼- represents PEGMA hydrogel crosslinked with Bis, and -●- represents PHMAA hydrogel crosslinked with Bis. Each data point represents the mean and standard deviation from four independent experiments.

The hydrogel stiffness quantified with an elastic-modulus measurement was significantly dependent on both $M_{X-linker}$ and the chemical structure of the crosslinker. Interestingly, the hydrogels crosslinked with MA were stiffer than those crosslinked with Bis, even at much lower $M_{X-linker}$ (Fig. 2a). The dependency of the elastic modulus on $M_{X-linker}$, as shown by the slopes of the linear-fitted curves, was also larger with the use of MA as a crosslinker, irrespective of the chemical structure of the gel-forming polymers (Table S1, Supporting Information). In contrast, the swelling ratios decreased with $M_{X-linker}$ were within almost the same range for both Bis and MA (Fig. S2, Supporting Information). The dependency of elastic modulus on swelling ratio was thus larger for both PEGMA and PHMAA hydrogels crosslinked with MA as compared with those crosslinked with Bis (Fig. S3, Supporting Information).

The number of elastically effective crosslinks of the hydrogel (N) was further calculated with the elastic modulus and swelling ratio using Equation 1, according to a rubber elasticity theory.

$$N = \frac{SQ^{-1/3}}{RT} \quad (1)$$

where S is the shear modulus calculated from the slope of σ versus $-(\lambda - \lambda^{-2})$ assuming the hydrogels followed an affined network model (σ : stress, λ : strain), and Q is the degree of swelling calculated using Equation 4 (see the Experimental Section).^[13] The N was larger for hydrogels crosslinked with MA than those crosslinked with Bis (Fig. 2b). Despite the higher stiffness resulting from the larger N , the hydrogel crosslinked with MA also presented a greater resistance to fracture than the hydrogel crosslinked with Bis by one order of magnitude (Fig. 2c).

2.3. Control of Hydrogel Degradation Rate and Protein-Release Kinetics Using OMA

The role of the crosslinker in regulating a hydrogel degradation rate independent of the initial elastic modulus of a hydrogel was examined using OMAs containing varied number of oxidized uronic acid residues. The hydrogel degradation was monitored with a decrease of the elastic modulus and an increase of the swelling ratio over time. The initial elastic modulus of the hydrogel was almost independent of the number of oxidized uronic acid residues (Fig. 3a). All hydrogels, including ones crosslinked with Bis, showed a decrease in the elastic modulus and an increase of the swelling ratio over time. Interestingly, hydrogels crosslinked with OMA showed a greater decrease of the elastic modulus and a greater increase of the swelling ratio than hydrogels crosslinked with Bis (Fig. 3b and c).

The degradation rate (k_1) was further calculated from the changes of the elastic modulus and swelling ratio using the first-order degradation kinetic equation (Equation 2, and Table S2 of the Supporting Information).

$$\frac{N_t}{N_0} = \exp(-k_1 t) \quad (2)$$

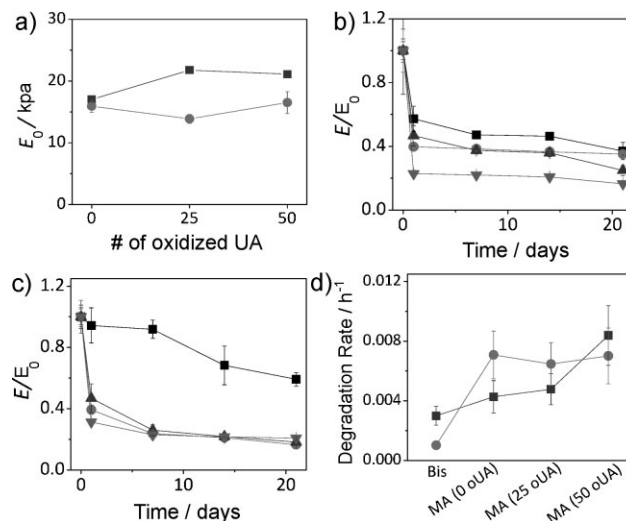


Figure 3. a) The initial elastic moduli (E_0) of both PEGMA (■) and PHMAA (●) hydrogels crosslinked with OMA are independent of the number of oxidized uronic acid (oUA) residues in the OMA. E_0 was measured after an hour of incubation in Dulbecco's Modified Eagle's Medium (DMEM). The hydrogel crosslinked with OMA showed the faster reduction in E for both b) PEGMA and c) PHMAA hydrogels. An increase in the number of oxidized uronic acid residues of the OMA further accelerated the decrease of E , specifically for PEGMA hydrogel. In (b) and (c), the E measured at each time point was normalized with E_0 . -●- represents hydrogel crosslinked with Bis, -■- represents hydrogel crosslinked with MA (0 oUA), -▲- represents hydrogel crosslinked with OMA containing 25 oxidized uronic acid residues (25 oUA), and -▼- represents hydrogel crosslinked with OMA containing 50 oxidized uronic acid residues (50 oUA). d) The degradation rate (k_1), calculated from the first-order kinetics (Equation 1) depends on the number of oxidized uronic acid residues in OMA. Each data point represents the mean and standard deviation from four independent experiments.

where N_t is the number of crosslinks at time t and N_0 is the number of crosslinks measured after one hour of buffer incubation.^[11b] Interestingly, independent of the initial hydrogel stiffness, k_1 was significantly larger with the use of OMA as a crosslinker as compared with a hydrogel crosslinked with Bis. The k_1 was further controlled by the number of oxidized uronic acid residues of OMA for both PEGMA and PHMAA gels. The dependency of k_1 on the number of oxidized uronic acid residues was more prominent with PEGMA gels (Fig. 3d).

The relevance of hydrogel degradation rate to the release rate of proteins encapsulated in the hydrogel was subsequently evaluated using bovine serum albumin (BSA) as a model therapeutic protein (Fig. 4a and b). Interestingly, hydrogels crosslinked with OMA facilitated the release of BSA from both PEGMA and PHMAA hydrogels, while the hydrogels crosslinked with MA or Bis limited the BSA release.

The release rate of BSA (k_2) was quantified by the amount of BSA diffused out of the hydrogel using the Ritger–Peppas equation (Equation 3) as a drug release model.

$$\frac{M_t}{M_\infty} = k_2 t^n \quad (3)$$

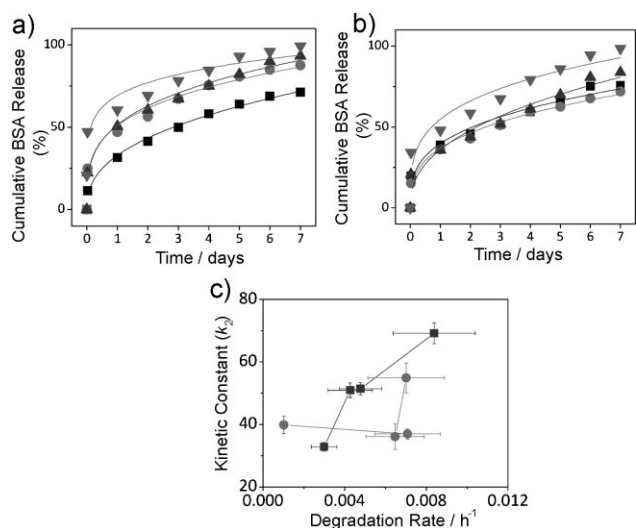


Figure 4. Protein release profiles of a) PEGMA and b) PHMAA hydrogels crosslinked with Bis or OMA. The BSA release was accelerated with increase of the number of oxidized uronic acid. In (a) and (b), -■- represents hydrogel crosslinked with Bis, -●- represents hydrogel crosslinked with MA (0 oUA), -▲- represents hydrogel crosslinked with OMA containing 25 oxidized uronic acid units (25 oUA), and -▼- represents hydrogel crosslinked with OMA containing 50 oxidized uronic acid units (50 oUA). c) The BSA release rates (k_2) increased with the hydrogel degradation rate. In (c), -■- represents PEGMA hydrogels and -●- represents PHMAA hydrogels.

where M_t/M_∞ is the fractional protein release at time t and n is the diffusional exponent related to the release mechanism.^[14,15] k_2 was dependent on the hydrogel degradation rate of hydrogel (k_1) for both PEGMA and PHMAA hydrogels, although the dependency of k_2 on k_1 was specific to the chemical structure of the gel-forming polymer (Fig. 4c, and Table S2, Supporting Information). k_2 was also dependent on the rate of hydrogel swelling, similar to the dependency of k_2 on k_1 (Fig. S4, Supporting Information). The n values for hydrogels crosslinked with Bis or OMA were between 0.2 and 0.5.

2.4. Controlling In Vivo Angiogenesis Using Angiogenic Growth Factor Encapsulated Hydrogels

Finally, the role of OMA in regulating hydrogel function to release angiogenic growth factors and subsequently promote the neovascularization in a connective tissue was evaluated. The vascular endothelial growth factor (VEGF) was encapsulated in PEGMA hydrogels crosslinked with Bis or OMA, and the VEGF-hydrogel construct was implanted on the chorioallantoic membrane (CAM) of chick embryos (Fig. S5a, Supporting Information).^[7,16–18] The implanted gel was gradually incorporated into the CAM within a day. Hydrogels incorporated into the CAM did not trigger any severe host inflammatory response as compared with a control tissue onto which no hydrogel was implanted (Fig. S5b, Supporting Information). The implantation of hydrogel containing VEGF resulted in an increase in the number of mature blood vessels marked with α -smooth muscle actin antibody (Fig. 5a).^[18]

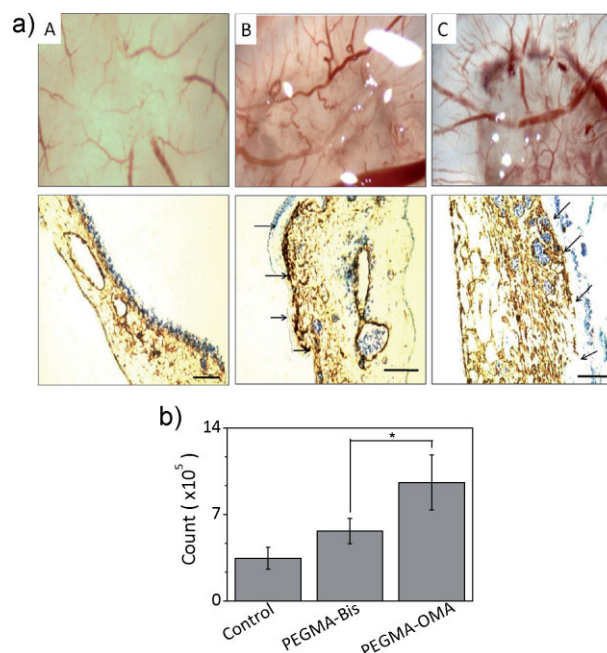


Figure 5. Chick embryo chorioallantoic membrane (CAM) angiogenesis assay. a) Implantation of hydrogel containing VEGF into the CAM significantly increased the blood vessel density (B, C) as compared with a negative control (A). The use of hydrogel crosslinked with OMA (C) (50 oxidized uronic acids per alginate chain, $M_{X-linker}$ of 0.01) as a VEGF delivery device further increased the blood vessel density as compared with the use of hydrogel crosslinked with Bis (B) ($M_{X-linker}$ of 0.6). No treatment was performed on the negative control. The upper photos show a top view of the CAM imaged with a CCD camera and the lower photos show a cross-section of the CAM imaged with antibody to α -smooth muscle actin (α -SMA). The mature capillary blood vessel was identified with α -SMA layer stained by the brown stain. The arrows indicate the CAM surface exposed to the hydrogel containing VEGF. b) The blood vessel density quantified from α -SMA staining was significantly higher with the use of hydrogel crosslinked with OMA as the VEGF delivery device. The difference of blood vessel density between the hydrogel crosslinked with Bis and the hydrogel crosslinked with OMA was statistically significant ($p^* < 0.05$). Each data point represents the mean and standard deviation from four independent experiments.

The hydrogel crosslinked with OMAs further increased the density of mature blood vessels, 1.5 times more than that crosslinked with Bis (Fig. 5b).

3. Discussion

This study demonstrated that the hydrolytically labile polymer crosslinker, OMA, enabled us to decouple the dependency between stiffness, toughness, and degradation rate of PEGMA and PHMAA hydrogels. Even with the smaller number of reactive groups, MA crosslinked both PEGMA and PHMAA to form stiffer and tougher hydrogels than those formed with a conventional small crosslinker, Bis. The polymer crosslinker modified to be hydrolytically labile, OMA, further enabled the control of hydrogel degradation rate and subsequent protein release rate while making

minimal changes in initial mechanical properties. Ultimately, the hydrogel crosslinked with OMA was successfully used as a VEGF-delivery device to enhance neovascularization in vivo.

Independent control of hydrogel stiffness and toughness could be achieved with the greater valency of methacrylic groups and longer chain length of MA than Bis. The finding that methacrylic alginate itself could not form a gel matrix within the concentration range used in this study confirmed that methacrylic alginate mostly acted as a crosslinker of PEGMA or PHMAA. The higher elastic modulus of the hydrogel crosslinked with MA compared to the hydrogel crosslinked with Bis indicated the larger number of elastically effective crosslinks of the hydrogel crosslinked with MA. The larger dependency of the elastic modulus on swelling ratio with hydrogels crosslinked with MA also confirmed the presence of a higher number of intermolecular crosslinks as compared to hydrogels crosslinked with Bis (Fig. S4, Supporting Information). It is well known that intramolecular crosslinks do not contribute to the elastic response of a hydrogel matrix, while they do affect the hydrogel swelling ratio.^[1b] It is also likely that energy being accumulated at a crosslinked junction of the gel during mechanical deformation is more readily dissipated through longer alginate chains, thus leading to greater fracture resistance.^[19]

The decoupled control of hydrogel stiffness and degradation rate was related to the capability of OMA to crosslink gel-forming polymers and its susceptibility to hydrolysis.^[11,12] The methacrylic OMA groups could initially crosslink pre-polymers or monomers to form an elastic gel network, irrespective of the number of oxidized uronic acid residues in the OMA groups. This result suggested that a potential decrease of the molecular weight of OMA due to oxidation did not affect initial hydrogel mechanical properties.

The hydrogel degradation rate was significantly controlled with the number of oxidized unit of OMA, irrespective of initial gel elastic moduli, as demonstrated with the dependency of a degradation rate (k_1) on the number of oxidized uronic acid residues of OMA (Fig. 3). It has been shown that hydrogels consisting of PEG or MA slowly degrade in a physiological condition, because of hydrolytic breakage of ester bonds between methacrylic groups and polymers.^[10c,22] Our study also showed that PEGMA hydrogels crosslinked with Bis or MA slowly degraded, likely due to hydrolysis of ester bonds, but PHMAA hydrogels crosslinked with Bis remained stable due to the absence of hydrolyzable groups. The degradation rates of the PEGMA-Bis and PEGMA-MA hydrogels could be further controlled with concentrations of PEGMA and methacrylic alginate. However, these approaches lead to significant changes of the initial elastic moduli of hydrogels. In contrast, the use of OMA could broaden the range of hydrogel degradation rate (k_1) independent of E_0 due to the minimal changes of initial number of crosslinks and hydrolytic chain breakage of OMA. k_1 increases with the number of oxidized unit of OMA.

The dependency of k_1 on the number of oxidized uronic acid residue was also mediated by the chemical structure of the gel-forming polymer. The smaller dependency of k_1 on the number of oxidized uronic acid residues with PHMAA hydrogel than PEGMA hydrogel is likely due to the significant chain relaxation of pendent PHMAA segments which affects the swelling ratio increase over time. However, this aspect needs to be further investigated in future studies.^[15]

The hydrogel degradation tuned with OMA further regulated the protein release rate (k_2) from the hydrogel as demonstrated with the increase of BSA release rate with the hydrogel degradation rate (k_1) by a factor of 7 (Fig. 4c). The protein release profile well fitted to the Ritger–Peppas transport model indicated that chain breakage of OMA in the hydrogel increased the gel permeability leading to the increase of protein diffusion rate.^[14,15] The dependency of k_2 on the hydrogel swelling ratio increase rate also suggested that the degradation of the hydrogels facilitated water diffusion into the hydrogel system, leading to faster release of protein (Fig. S4, Supporting Information). The protein release rate are further accelerated with an increase of the number of oxidized uronic acid residues in OMA. In a similar manner, the hydrogel crosslinked with OMA likely released a larger amount of VEGF than the gel crosslinked with Bis within a given time, thus amplifying the VEGF-induced signal transduction to stimulate angiogenesis.^[17–19]

The control of protein release rate from a biodegradable hydrogel has been previously demonstrated using various biodegradable hydrogel systems. However, the protein release rate of most hydrogels is dependent on the initial elastic moduli. In contrast, the hydrogel prepared using the OMA as a crosslinker allowed the control of protein release rate over a broad range without altering E_0 . This decoupled control of the initial hydrogel mechanics and the degradation rate will therefore enable us to implant a protein-releasing hydrogel in tissue subject to mechanical loading and to subsequently attain a desired protein release profile.

Overall, the results of this study provide a novel strategy to control mechanical properties and degradation rate of a hydrogel in an independent manner. The ability of polymer crosslinker to regulate gel properties can be further tuned with several other molecular parameters such as molecular weight and number of methacrylic groups linked to a polymer. This polymer crosslinker will be broadly useful in controlling properties and function of a broad array of hydrogel system used in various biomedical applications including tissue engineering, drug delivery, and cell therapies.^[1] In addition, the strategy to synthesize polymer crosslinker could be readily used to prepare a wide array of polymer crosslinker including polysaccharide or polypeptide derivatives.

4. Conclusions

This study demonstrated that the biodegradable polymer crosslinker, OMA, played a critical role in regulating stiffness, toughness, and degradation rate of hydrogels in an independent manner. Specifically, hydrogels crosslinked with methacrylic alginate presented higher stiffness and toughness than those crosslinked with a short crosslinker, due to the larger number of crosslinks and enhanced fracture energy dissipation of the gel network. Furthermore, the use of OMA as a crosslinker allowed us to tune the hydrogel degradation rate with the degree of oxidation while minimally changing initial hydrogel stiffness. This refined control of hydrogel degradation rate was related to the independency of the initial number of elastically effective crosslinks and the dependency of gel degradation rate on the number of oxidized uronic acid residues of OMA. Therefore, the hydrogel crosslinked

with OMA could be used as a device to release proteins in a sustained manner and subsequently improve vascular network formation *in vivo*. Taken together, the OMA would be highly useful to controlling the properties of a broad array of hydrogels and expediting the use of hydrogels in various biological applications.

5. Experimental

Modification of Alginate Molecules: The alginate used in this experiment (molecular weight (M_w) \approx 100 000) was obtained by irradiating alginate rich in gluronic acid residues, (LF20/40, FMC Technologies, $M_w \approx$ 250 000) with a dose of 2 Mrad for 4 hours from a ^{60}Co source [20]. The oxidized methacrylic alginate (OMA) was prepared by mixing an alginate solution with NaIO_4 (Sigma–Aldrich) for 18 hours with stirring [11]. The reaction was quenched with ethylene glycol, and the mixture was dialyzed extensively for one day, changing the deionized (DI) water twice. The molar ratio between NaIO_4 and uronic acid residue of alginate was varied from 0.05 to 0.10. The oxidized alginate was next dissolved in a 0.1 M MES (2-(*N*-morpholino) ethanesulfonic acid) buffer (pH 6.4, Sigma–Aldrich) at a concentration of 10% (w/w) to prepare methacrylic alginate. For the synthesis of methacrylic alginate (MA), non-oxidized alginate was dissolved in the same MES buffer. Then, 1-hydroxybenzotriazole (HOBt, Sigma–Aldrich), 1-ethyl-3-(3-dimethylaminopropyl) carbodiimide (EDC, Thermo Scientific), and 2-aminoethyl methacrylate (MA-NH_2 , Sigma–Aldrich) were added to the alginate solution and the mixture was subject to stirring for 18 hours. Both the molar ratios of HOBt to MA-NH_2 and EDC to MA-NH_2 were kept constant at 2:1. The mixture was dialyzed extensively for two days, while exchanging the DI water every 12 hours. All the alginate samples were lyophilized, and the dried samples were redissolved in DI water to reconstitute them to 3% (w/w) solution. The substitution degrees of methacrylic groups of OMA and MA were determined with $^1\text{H-NMR}$ spectra (300MHz, QE300, General Electric).

Hydrogel Preparation and Characterization: Poly (ethylene glycol) methacrylate (PEGMA, $M_n \approx$ 526, Sigma–Aldrich) and *N*-hydroxymethylacrylamide (HMAA, Sigma–Aldrich) were dissolved in DI water at concentrations of 10% and 4% (w/w), respectively. One of two crosslinkers, *N,N'*-methylenebisacrylamide (Bis, Sigma–Aldrich) or MA was also dissolved in DI water at a concentration of 3% (w/w). The pre-gelled solution was made by mixing 1 mL of the PEGMA or HMAA solution with varied amounts of crosslinker solutions (50, 100, 200, and 300 μL) while keeping the total gel-forming PEGMA or HMAA concentrations constant at 7.7% and 3.1% (w/w), respectively. The 1 mL of pre-gelled solution was mixed with 1 M ammonium persulfate (40 μL , Sigma–Aldrich) as an initiator and *N,N,N',N'*-tetramethylethylenediamine (5 μL , Sigma–Aldrich) as a catalyst. The gels were cured between glass plates with spacers of 1-mm thickness. Gel disks with a diameter of 10 mm were punched out and subjected to compression with a mechanical testing system (MTS Insight). The elastic modulus was calculated from the slope of a stress (σ) versus strain (λ) curve at the first 10% strain. The degree of swelling (Q) was calculated using the following equation

$$Q = v^{-2} = \rho_p \left[\frac{Q_m}{\rho_s} + \frac{1}{\rho_p} \right] \quad (4)$$

where ρ_s is the density of water, ρ_p is the density of polymer, and Q_m is the swelling ratio: the mass ratio of swelled gel to the dried gel.

The hydrogel resistance to fracture was measured using gels cut into thin rectangular strips (10 mm \times 30 mm \times 1 mm). Each end of the gel strip was glued to a small steel sheet on which a tensile grip set was attached. A small notch, 1 mm from the edge, was created on each side in the middle of the gel strip to localize the tensile force and fracture in the middle, not at the gripping points. The Young's modulus was calculated from the slope of stress (σ) versus strain (λ) curve and the work done by tensile deformation

(W_T) was calculated from the area under the curve divided by the volume of the gel [21].

Hydrogel Degradation: Hydrogel made with Bis or OMA was incubated in Dulbecco's Modified Eagle Medium (pH 7.4, Invitrogen) at 37 °C. The medium was changed once per week until the measurements were discontinued. Elastic modulus and swelling ratio were measured over time and the number of crosslinks (N) was subsequently calculated using Equation 1.

Protein Release Studies: Bovine serum albumin (BSA, Sigma) was mixed with the pre-gel solution prior to the crosslinking reaction, so the BSA could be encapsulated in the hydrogel *in situ*. A gel disk was incubated in phosphate buffer saline (PBS; pH 7.4) at 37 °C, while keeping the samples sterile. A sample was taken every day for one week. Then, the gel was incubated in the medium for additional days until no detectable amount was observed to quantify the total protein. The amount of BSA released from the hydrogel was determined by using a BCA Assay Kit (Thermo Scientific), according to the manufacturer's instructions. The amount of BSA released from the hydrogel was divided by the amount of BSA initially encapsulated into the hydrogel to calculate the cumulative percentage of BSA released. The release profile was analyzed using the Ritger–Peppas equation as a drug release model (Equation 3) [14,15].

In Vivo VEGF Release Study Using Chick Embryo Chorioallantoic Membrane (CAM): The CAM angiogenesis assay was performed according to a previously developed method (Fig. S5a, Supporting Information) [7]. Briefly, embryonic chicken eggs (Hy-Line W-36) were purchased from the Poultry Research Farm at the University of Illinois (Urbana, IL). The eggs were incubated at 37 °C with 5% CO_2 . On the 9th day of gestation, a small window (1 cm \times 1 cm) was created on top of each egg. After two days of additional incubation to stabilize CAM and the embryos, a gel disk (5-mm diameter, 1-mm thickness) containing vascular endothelial growth factor (VEGF)-165 (30 ng per gel disk, R&D systems) was implanted on top of the CAM. After incubation for four days, the membrane was fixed with 10% neutral buffered formalin (NBF) for 20 hours. The fixed membrane surrounding the gel disk (10 mm \times 10 mm) was cut out. The collected tissue was processed for paraffin embedding, and the cross-section was stained with standard Hematoxylin & Eosin (H&E) for the histological analysis. Another section from the same tissue sample was stained for α -smooth muscle actin (α -SMA Immunohistology Kit, Sigma–Aldrich) to count the number of mature blood vessels [17]. Images were captured with a CCD camera (Leica D-LUX 3) mounted on an inverted microscope (Leica DMIL). The blood vessels were quantified by counting the α -SMA stained pixels using ImageJ (free software available from NIH, <http://rsbweb.nih.gov/ij/>, last accessed July 2009). Each condition was tested in triplicate. Statistical significance between two data populations was evaluated using an unpaired, two-tailed Student's *t*-test in Microsoft Excel. Differences were considered statistically significant for $p < 0.05$.

Acknowledgements

This work was funded by American Heart Association Scientist Development Grant (0830468Z) and US Army Grant (W81XWH-08-1-0701). The authors also wish to thank Chet Utterback at the University of Illinois Poultry Research Farm (Urbana, IL) for the supply of embryonic chicken eggs and equipments. Supporting Information is available online from Wiley InterScience or from the author.

Received: May 18, 2009
Published online: August 19, 2009

- [1] a) B. D. Ratner, A. S. Hoffman, in *Hydrogels for Medical and Related Applications*, Vol. 31 (Ed: J. D. Andrade), ACS, Washington, DC 1976.
b) L. E. Nielsen, *Polym. Rev.* **1969**, 3, 69.
[2] K. Y. Lee, D. J. Mooney, *Chem. Rev.* **2001**, 101, 1869.

- [3] N. A. Peppas, J. Z. Hilt, A. Khademhosseini, R. Langer, *Adv. Mater.* **2006**, *18*, 1345.
- [4] L. E. Nielsen, R. F. Landel, *Mechanical Properties of Polymers and Composites*, 2nd ed. Marcel Dekker, New York **1994**, chapter 5.
- [5] A. B. Clayton, T. V. Chirila, X. Lou, *Polym. Int.* **1997**, *44*, 201.
- [6] X. Lou, T. V. Chirila, *J. Biomater. Appl.* **1999**, *14*, 184.
- [7] C. A. Staton, C. Lewis, R. Bicknell, *Angiogenesis Assays: A Critical Appraisal of Current Techniques*, Wiley, New York **2007**, Chapter 11.
- [8] a) J. P. Gong, Y. Katsuyama, T. Kurokawa, Y. Osada, *Adv. Mater.* **2003**, *15*, 1155. b) Y. Okumura, K. Ito, *Adv. Mater.* **2001**, *13*, 485. c) K. Haraguchi, T. Takehisa, *Adv. Mater.* **2002**, *14*, 1120.
- [9] a) G. T. Hermanson, in *Bioconjugate Techniques*, Academic, San Diego, CA, USA **1996**, p. 169. b) J. A. Rowley, G. Madlambayan, D. J. Mooney, *Biomaterials*, **1999**, *20*, 45.
- [10] a) H. J. Kong, M. K. Smith, D. J. Mooney, *Biomaterials* **2003**, *24*, 4023. b) P. Bulpitt, D. Aeschlimann, *J. Biomed. Mater. Res.* **1999**, *47*, 152. c) O. Jeon, K. H. Bouhadir, J. M. Mansour, E. Alsberg, *Biomaterials* **2009**, *30*, 2724.
- [11] a) T. Boontheekul, H. J. Kong, D. J. Mooney, *Biomaterials*. **2005**, *26*, 2455. b) H. J. Kong, D. Kaigler, K. Kim, D. J. Mooney, *Biomacromolecules* **2004**, *5*, 1720.
- [12] K. H. Bouhadir, D. S. Hausman, D. J. Mooney, *Polymer* **1999**, *40*, 3575.
- [13] H. J. Kong, E. Alsberg, D. Kaigler, K. Y. Lee, D. J. Mooney, *Adv. Mater.* **2004**, *16*, 1917.
- [14] P. L. Ritger, N. A. Peppas, *J. Controlled Release* **1987**, *5*, 23.
- [15] L. Serra, J. Domenech, N. A. Peppas, *Biomaterials* **2006**, *27*, 5440.
- [16] J. Borges, F. T. Tegtmeier, N. T. Padron, M. C. Mueller, E. V. Lang, G. B. Stark, *Tissue Eng.* **2003**, *9*, 441.
- [17] J. Wilting, B. Christ, M. Bokeloh, H. Weich, *Cell Tissue Res.* **1993**, *274*, 163.
- [18] J. Sung, P. W. Barone, H. J. Kong, M. J. Strano, *Biomaterials* **2009**, *30*, 622.
- [19] W. M. Saltzman, *Drug Delivery: Engineering Principles for Drug Therapy*, Oxford University Press, New York **2001**, Ch. 9.
- [20] H. J. Kong, M. K. Smith, D. J. Mooney, *Biomaterials* **2003**, *24*, 4023.
- [21] H. J. Kong, E. Wong, D. J. Mooney, *Macromolecules* **2003**, *36*, 4582.
- [22] a) A. Sawhney, C. Pathak, J. Hubbell, *Macromolecules* **1993**, *26*, 581. b) D. Elbert, J. A. Hubbel, *Biomacromolecules* **2001**, *2*, 430.